Task-Space Control of Robot Manipulators With Null-Space Compliance

Hamid Sadeghian, Luigi Villani, *Senior Member, IEEE*, Mehdi Keshmiri, and Bruno Siciliano, *Fellow, IEEE*

***Abstract*—In this paper, the problem of controlling a robot manipulator in task space, while guaranteeing a compliant behavior for the redundant degrees of freedom, is considered. This issue may arise in the case where the robot experiences an interaction on its body, especially in the presence of humans. The proposed approach guarantees correct task execution and compliance of the robot's body during intentional or accidental interaction in the null space of the main task, simultaneously. The asymptotic stability of the task-space error is ensured by using suitable observers to estimate and compensate the generalized forces acting on the task variables, without using joint torque measurements. Two different controller–observer algorithms are designed, and they are based on the task-space error and on the generalized momentum of the robot, respectively. The performance of the proposed algorithms is verified in experiments on a 7R lightweight robot arm.**

***Index Terms*—Disturbance observer, null-space compliance, task-space control.**

I. Introduction

NEW applications where robots are employed near humans are growing rapidly. Unlike the industrial robots, which are stiff to guarantee high precision, the robots used in anthropic environments must be designed with high degree of compliance to ensure safety. This is especially true for the applications requiring physical human–robot interaction [2], not only because of unexpected impacts of robots with humans but for the execution of collaborative tasks requiring intentional exchange of forces as well.

A safe human–robot coexistence can be guaranteed combining different strategies. The safest approach is to avoid any unwanted collisions. This, however, can be achieved using exteroceptive sensors such as cameras that are ineffective in the case of fast interaction. Hence, appropriate collision detection and reaction strategies must be adopted [3]. A possibility is that to cover the manipulator body with a sensitive skin to detect and/or measure the interaction forces. Alternatively, suitable observers can be used to estimate the collision forces from joint positions or torques [4], [5]. For this purpose, an effective approach based on the computation of the generalized momentum of the robot, without using any torque sensors, was proposed in [6]. The reaction strategies are aimed at immediately removing the robot from the collision area. Nevertheless, in the case of redundant robots, it is possible to preserve as much as possible the execution of the end effector task by projecting the reaction torques into the null space of the main task [7].

Robot compliance is useful in order to reduce the interaction forces, both in the case of collision and during physical collaboration between humans and robots [8]. Compliance can be introduced passively by using elastic decoupling between the actuator and the driven link with fixed or variable joint stiffness [9] or actively by relying on fast control loops [10].

Impedance control represents an effective approach to control actively the robot's compliance. The impedance behavior usually is given to the task variables to control the interaction of the end effector [11]–[13], also during the execution of visual servoing tasks [14]. However, an active compliance behavior can be also imposed to the joint variables to enhance safety [15]–[18]. The Cartesian impedance control for torque controlled flexible joint and redundant robots was investigated thoroughly in [19]. The impedance control problem with null-space stiffness control for 7 degree-of-freedom (DOF) flexible joint arms, based on singular perturbation approach and passivity based approach was addressed in [20] and [21], respectively.

Recently, problems and solutions related to kinematic redundancy have gained new interest because of the application of robotic systems with a high number of DOFs, such as humanoid and dual-arm robots. A theoretical and empirical evaluation of different operational space control techniques for redundant manipulators has been presented in [22]. A well-established framework to deal with highly redundant robots is multipriority control, which can be performed both at the kinematic [23], [24] and dynamic levels [25], [26]. Within this framework, it is possible to control the behavior of several interaction points on the body of the robot.

Multipriority Cartesian impedance control has been investigated in [27], where multiple impedances with a specified order of priority are realized in the Cartesian space. A similar approach has been proposed in [28] and [29] to achieve an impedance control for the joint variables in the null space of a Cartesian impedance control imposed to the end effector.

Manuscript received July 3, 2013; accepted November 14, 2013. Date of publication December 13, 2013; date of current version April 1, 2014. This paper was recommended for publication by Associate Editor Y. Choi and Editor B. J. Nelson upon evaluation of the reviewers' comments. A preliminary version of this paper was published in the *proceedings of the IEEE/RSJ International Conference on Intelligent Robots and Systems, 2012* [1]. The conference paper contains only the main idea without stability proof and experiments. This work was supported in part by the Italian Ministry of University and Research within the PRIN 2009 20094WTJ29_003 ROCOCO' Project and by the European Community within the FP7 ICT-287513 SAPHARI Project.

H. Sadeghian is with the Department of Biomedical Engineering, Faculty of Engineering, University of Isfahan, Isfahan 8174673441, Iran (e-mail: h.sadeghian@eng.ui.ac.ir).

L. Villani and B. Siciliano are with the Department of Electrical Engineering and Information Technology, University of Naples Federico II, Naples 80138, Italy (e-mail: lvillani@unina.it; siciliano@ieee.org).

M. Keshmiri is with the Department of Mechanical Engineering, Isfahan University of Technology, Isfahan 8415683111, Iran (e-mail: mehdik@cc.iut.ac.ir).

Color versions of one or more of the figures in this paper are available online at http://ieeexplore.ieee.org.

Digital Object Identifier 10.1109/TRO.2013.2291630

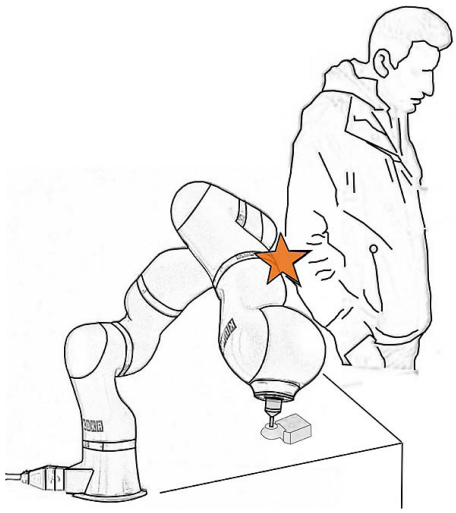

Fig. 1. Robot working close to a human.

The problem of multipoint human robot interaction was considered in [16]. In [17] and [18], a model-free and an iterative learning impedance control were proposed to deal with uncertainties and torque measurement noises.

When dealing with null-space control, an important issue is the representation of the null-space dynamics. In [30], a set of minimal variables is used to describe the null-space motion. These variables are called null-space velocities, and they are defined by means of a null-space base matrix. The null-space velocities are in general nonintegrable [31], and, thus, the design of a null-space compliance controller is not straightforward. This problem was solved in [32] by using a semidefinite Lyapunov function.

The null-space impedance as a result of multipriority control in acceleration level was presented in [26]. The approach was motivated by the need of having control over the interaction of the robot body with the environment in the joint space in spite of the task-space control. It was shown that, in order to ensure impedance behavior as the secondary task without affecting the main task, the external forces acting on the main task variables must be suitably compensated by the controller. This is possible, e.g., if the external torques are measured [15], [33] or estimated [4]. Notice that the correct execution of the robot's main task during the interaction, although subordinated to safety, is also appealing and important.

This paper considers the problem of controlling a robot manipulator in the task space, while ensuring a compliant behavior for the redundant DOFs in the joint space. An example of application scenario is depicted in Fig. 1, where a robot working on a table experiences a contact with a human. This contact may produce errors on the main task of the robot if active compliance is used to achieve a safe interaction. Our goal is to minimize the error of the main task and at the same time to ensure safe interaction through active compliance in the null space of the main task.

To this purpose, two control approaches which do not require direct joint torque measurements are proposed. The first approach is based on a disturbance observer which estimates the external forces acting on the main task variables on the basis of the task-space error. The second approach relies on the momentum-based observer [3]. In both cases, the overall stability of the system, with asymptotic convergence of the main task and a desired impedance behavior in the null space of the main task, is proven through a rigorous analysis. A number of experiments are presented for a 7-DOF KUKA LWR4 robot.

This paper is organized as follows. The joint impedance and null-space impedance concepts are reviewed in Section II. The main results of the paper including the task error-based disturbance observer and momentum-based observer are proposed in Sections III and IV, respectively. In Section V, the performance of the proposed schemes is evaluated experimentally. Conclusions are drawn in Section VI.

II. Preliminaries

A. System Description

The dynamic model of a n-link robot manipulator can be written as

$$\boldsymbol{M}(\boldsymbol{q})\ddot{\boldsymbol{q}} + \boldsymbol{C}(\boldsymbol{q},\dot{\boldsymbol{q}})\dot{\boldsymbol{q}} + \boldsymbol{g}(\boldsymbol{q}) + \boldsymbol{\tau}_{\text{ext}} = \boldsymbol{\tau} \tag{1}$$

where $\boldsymbol{q}$ is the $(n \times 1)$ joint vector, $\boldsymbol{M}(\boldsymbol{q})$ is $(n \times n)$ inertia matrix, $\boldsymbol{C}(\boldsymbol{q},\dot{\boldsymbol{q}})\dot{\boldsymbol{q}}$ is the $(n \times 1)$ vector of Coriolis and centrifugal torques, and $\boldsymbol{g}(\boldsymbol{q})$ is the $(n \times 1)$ vector of the gravitational torques. Furthermore, $\boldsymbol{\tau}$ is the $(n \times 1)$ vector of control torques, and $\boldsymbol{\tau}_{\text{ext}}$ is the $(n \times 1)$ vector of external torques resulting from the interaction with the environment. If the manipulator is equipped with torque sensors in its joints or force sensors on the interaction points, these external torques can be directly measured.

B. Joint Space Impedance Control

Impedance control is one of the most adopted methods of controlling the interaction between a manipulator and the environment. While the Cartesian or task-space impedance control regulates the mechanical impedance of the robot end effector [34], the joint space impedance control guarantees a compliant behavior of the robot joints. The joint space impedance equations are

$$\boldsymbol{M}_d(\ddot{\boldsymbol{q}}_d - \ddot{\boldsymbol{q}}) + \boldsymbol{B}_d(\dot{\boldsymbol{q}}_d - \dot{\boldsymbol{q}}) + \boldsymbol{K}_d(\boldsymbol{q}_d - \boldsymbol{q}) = \boldsymbol{\tau}_{\text{ext}} \tag{2}$$

where $\boldsymbol{q}_d(t)$ is a desired trajectory, while $\boldsymbol{M}_d$, $\boldsymbol{B}_d$, and $\boldsymbol{K}_d$ are $(n \times n)$ positive-definite matrices, representing the desired inertia, damping, and stiffness, respectively.

The impedance behavior (2), with a freely chosen desired inertia matrix $\boldsymbol{M}_d$, can be achieved only if a measure or estimation of the external torque is available and is used in the feedback control law. Namely, we have the following control law:

$$\boldsymbol{\tau} = \boldsymbol{M}(\boldsymbol{q})\ddot{\boldsymbol{q}}_c + \boldsymbol{C}(\boldsymbol{q},\dot{\boldsymbol{q}})\dot{\boldsymbol{q}} + \boldsymbol{g}(\boldsymbol{q}) + \boldsymbol{\tau}_{\text{ext}} \tag{3}$$

with the command joint acceleration $\ddot{\boldsymbol{q}}_c$ chosen as

$$\ddot{\boldsymbol{q}}_c = \ddot{\boldsymbol{q}}_d + \boldsymbol{M}_d^{-1}(\boldsymbol{B}_d\dot{\tilde{\boldsymbol{q}}} + \boldsymbol{K}_d\tilde{\boldsymbol{q}} - \boldsymbol{\tau}_{\text{ext}}) \tag{4}$$

where $\tilde{\boldsymbol{q}} = \boldsymbol{q}_d - \boldsymbol{q}$ leads to the closed loop dynamics (2).

In the case that $\boldsymbol{\tau}_{\rm ext}$ is not available or is not used in the controller, the joint impedance behavior (2) can be achieved only with $\boldsymbol{M}_d = \boldsymbol{M}(\boldsymbol{q})$, using the control law

$$\boldsymbol{\tau} = \boldsymbol{M}(\boldsymbol{q})\ddot{\boldsymbol{q}}_d + \boldsymbol{B}_d\dot{\tilde{\boldsymbol{q}}} + \boldsymbol{K}_d\tilde{\boldsymbol{q}} + \boldsymbol{C}(\boldsymbol{q},\dot{\boldsymbol{q}})\dot{\boldsymbol{q}} + \boldsymbol{g}(\boldsymbol{q}). \quad (5)$$

Notice that the joint space impedance control can be applied to both redundant and nonredundant manipulators, since it is achieved in the joint space.

C. Null-Space Impedance Control

For a redundant manipulator, it is possible to have some kind of joint impedance and task-space impedance simultaneously. Namely, a joint space impedance can be achieved in the null space of the main task, usually assigned to end-effector coordinates, as a result of a multipriority redundancy resolution control [25], [26]. Using this approach, it is possible to control the interaction both on the end effector and on the robot body.

Let us denote the task-space variable with the $(m \times 1)$ vector $\boldsymbol{x}$, with $m < n$. The relation between joint and task velocities are given through $(m \times n)$ Jacobian matrix $\boldsymbol{J}(\boldsymbol{q})$ as

$$\dot{\boldsymbol{x}} = \boldsymbol{J}\dot{\boldsymbol{q}}. \quad (6)$$

A general solution to (6) is given by

$$\dot{\boldsymbol{q}} = \boldsymbol{J}^{\dagger}\dot{\boldsymbol{x}} + \boldsymbol{N}\dot{\boldsymbol{q}} \quad (7)$$

where $\boldsymbol{J}^{\dagger}(\boldsymbol{q})$ is any $(n \times m)$ generalized inverse of $\boldsymbol{J}$ and $\boldsymbol{N}$ is a $(n \times n)$ matrix which projects $\dot{\boldsymbol{q}}$ to the null space of $\boldsymbol{J}$. A general form of the null-space projection matrix is given by

$$\boldsymbol{N} = \boldsymbol{I} - \boldsymbol{J}^{\dagger}\boldsymbol{J}. \quad (8)$$

In this paper, it is assumed that the robot always moves in a region of the configuration space free of kinematic singularities, i.e., the Jacobian matrix is always of full rank m.

While (7) resolves the redundancy of the system at velocity level, solving redundancy at acceleration level is more elaborate and provides a joint acceleration solution for a given task acceleration [26].

In the case that the measure of the external torque $\boldsymbol{\tau}_{\rm ext}$ is available, a null-space impedance behavior can be achieved by using the control law (3) with the $(n \times 1)$ command joint acceleration

$$\ddot{\boldsymbol{q}}_c = \boldsymbol{J}^{\dagger}(\ddot{\boldsymbol{x}}_c - \dot{\boldsymbol{J}}\dot{\boldsymbol{q}}) + \boldsymbol{N}(\ddot{\boldsymbol{q}}_d + \boldsymbol{M}_d^{-1}(\boldsymbol{B}_d\dot{\tilde{\boldsymbol{q}}} + \boldsymbol{K}_d\tilde{\boldsymbol{q}} - \boldsymbol{\tau}_{\rm ext})). \quad (9)$$

Here, $\ddot{\boldsymbol{x}}_c$ is the $(m \times 1)$ command acceleration in the task space. With standard mathematical calculations, the following task space and null-space closed-loop dynamics are derived:

$$\ddot{\boldsymbol{x}} = \ddot{\boldsymbol{x}}_c \quad (10)$$

$$\boldsymbol{N}(\ddot{\tilde{\boldsymbol{q}}} + \boldsymbol{M}_d^{-1}(\boldsymbol{B}_d\dot{\tilde{\boldsymbol{q}}} + \boldsymbol{K}_d\tilde{\boldsymbol{q}} - \boldsymbol{\tau}_{\rm ext})) = \boldsymbol{0}. \quad (11)$$

Thus, at acceleration level, the task-space dynamics (10) is decoupled from the null-space dynamics (11). In particular, (11) represents an impedance equation expressed in terms of joint variables, projected in the null space. By a proper choice of the null-space impedance matrices, it is possible to achieve a desired compliant behavior for the robot body, without affecting the task-space dynamics.

When the external torque information is not available, the control torque (3) and the command acceleration (9) can be computed with $\boldsymbol{\tau}_{\rm ext} = \boldsymbol{0}$. Hence, the following closed-loop equations are obtained in place of (10) and (11):

$$\ddot{\boldsymbol{x}} = \ddot{\boldsymbol{x}}_c - \boldsymbol{J}\boldsymbol{M}^{-1}\boldsymbol{\tau}_{\rm ext} \quad (12)$$

$$\boldsymbol{N}(\ddot{\tilde{\boldsymbol{q}}} + \boldsymbol{M}_d^{-1}(\boldsymbol{B}_d\dot{\tilde{\boldsymbol{q}}} + \boldsymbol{K}_d\tilde{\boldsymbol{q}}) - \boldsymbol{M}^{-1}\boldsymbol{\tau}_{\rm ext}) = \boldsymbol{0}. \quad (13)$$

Differently from (10), the task-space acceleration (12) is affected by the external torque $\boldsymbol{\tau}_{\rm ext}$. Moreover, the null-space dynamics (13) is a projected impedance equation as in (11) only if the mass matrix $\boldsymbol{M}_d$ is set as the inertia matrix of the robot, i.e., $\boldsymbol{M}_d = \boldsymbol{M}(\boldsymbol{q})$.

An important role in the null-space dynamics (13) is played by the dynamically consistent generalized inverse [35]

$$\boldsymbol{J}^{\#}(\boldsymbol{q}) = \boldsymbol{M}^{-1}\boldsymbol{J}^T(\boldsymbol{J}\boldsymbol{M}^{-1}\boldsymbol{J}^T)^{-1}. \quad (14)$$

In detail, by using $\boldsymbol{J}^{\#}$ and the corresponding null-space projector $\boldsymbol{N}_{\#} = \boldsymbol{I} - \boldsymbol{J}^{\#}\boldsymbol{J}$ in the command acceleration (9) (with $\boldsymbol{M}_d = \boldsymbol{M}$ and $\boldsymbol{\tau}_{\rm ext} = \boldsymbol{0}$), the following equation is achieved in place of (13):

$$\boldsymbol{N}_{\#}\left(\ddot{\tilde{\boldsymbol{q}}} + \boldsymbol{M}^{-1}(\boldsymbol{B}_d\dot{\tilde{\boldsymbol{q}}} + \boldsymbol{K}_d\tilde{\boldsymbol{q}} - \boldsymbol{\tau}_{\rm ext})\right) = \boldsymbol{0}. \quad (15)$$

If the external interaction happens only at the end effector, i.e., $\boldsymbol{\tau}_{\rm ext} = \boldsymbol{J}^T\boldsymbol{F}_{\rm ext}$, the null-space closed-loop dynamics (13) is not affected by these forces, being $\boldsymbol{N}_{\#}\boldsymbol{M}^{-1}\boldsymbol{J}^T\boldsymbol{F}_{\rm ext} = \boldsymbol{0}$. This is not true when a generic generalized inverse is used.

Equation (15) represents the impedance behavior projected in the null space, with dimension $r = n - m$, through n equations that, therefore, are not all independent. This problem can be overcome by considering a $(n \times r)$ matrix $\boldsymbol{Z}(\boldsymbol{q})$, such that $\boldsymbol{J}\boldsymbol{Z} = \boldsymbol{0}$, and introducing a $(r \times 1)$ velocity vector $\boldsymbol{\nu}$, such that

$$\dot{\boldsymbol{q}}_n = \boldsymbol{N}\dot{\boldsymbol{q}} = \boldsymbol{Z}\boldsymbol{\nu}. \quad (16)$$

As shown in [30], a convenient choice of $\boldsymbol{\nu}$ based on (16) is given by left inertia-weighted generalized inverse $\boldsymbol{\nu} = \boldsymbol{Z}^{\#}\dot{\boldsymbol{q}} = (\boldsymbol{Z}^T\boldsymbol{M}\boldsymbol{Z})^{-1}\boldsymbol{Z}^T\boldsymbol{M}\dot{\boldsymbol{q}}$. By this choice, the extended Jacobian matrix $\boldsymbol{J}_E(\boldsymbol{q})$ is defined as

$$\begin{pmatrix}\dot{\boldsymbol{x}}\\ \boldsymbol{\nu}\end{pmatrix} = \boldsymbol{J}_E(\boldsymbol{q})\dot{\boldsymbol{q}} = \begin{pmatrix}\boldsymbol{J}(\boldsymbol{q})\\ \boldsymbol{Z}^{\#}(\boldsymbol{q})\end{pmatrix}\dot{\boldsymbol{q}} \quad (17)$$

is nonsingular for full-rank matrix $\boldsymbol{J}$, and the inverse is

$$\boldsymbol{J}_E^{-1}(\boldsymbol{q}) = \left[\boldsymbol{J}^{\#}(\boldsymbol{q}) \;\; \boldsymbol{Z}(\boldsymbol{q})\right]. \quad (18)$$

In view of (17) and (18), the following decomposition for the joint velocity holds:

$$\dot{\boldsymbol{q}} = \boldsymbol{J}^{\#}\dot{\boldsymbol{x}} + \boldsymbol{Z}\boldsymbol{\nu}. \quad (19)$$

Because of the unique relationship between the task space and the null-space variables with the joint space variables given by (17) and (19), it is possible to project the dynamics equation (1) both in the task space and the null space. The complete dynamic model in the task and null space, and its most relevant properties for the control design are illustrated in Appendix A.

It is worth observing that a special care must be taken for the computation of $\boldsymbol{Z}(\boldsymbol{q})$ [19]. In fact, numerical calculation of this matrix, based on the singular value decomposition method, may

cause discontinuity in the solution. Thus, the numerical stability of the system is subjected to the choice of this matrix, which is not unique [36].

Based on (17) and (19), the second-order inverse kinematics solution for the command acceleration can be written as

$$\ddot{\boldsymbol{q}}_c = \boldsymbol{J}_E^{-1}\left(\begin{pmatrix}\ddot{\boldsymbol{x}}_c\\ \dot{\boldsymbol{\nu}}_c\end{pmatrix} - \dot{\boldsymbol{J}}_E\dot{\boldsymbol{q}}\right) = \boldsymbol{J}^{\#}(\ddot{\boldsymbol{x}}_c - \dot{\boldsymbol{J}}\dot{\boldsymbol{q}}) + \boldsymbol{Z}(\dot{\boldsymbol{\nu}}_c - \dot{\boldsymbol{Z}}^{\#}\dot{\boldsymbol{q}}). \tag{20}$$

By using the aforementioned command acceleration in the control law

$$\boldsymbol{\tau} = \boldsymbol{M}(\boldsymbol{q})\ddot{\boldsymbol{q}}_c + \boldsymbol{C}(\boldsymbol{q},\dot{\boldsymbol{q}})\dot{\boldsymbol{q}} + \boldsymbol{g}(\boldsymbol{q}) \tag{21}$$

for the system (1), the closed-loop dynamics can be written as

$$\ddot{\boldsymbol{q}} = \boldsymbol{J}^{\#}(\ddot{\boldsymbol{x}}_c - \dot{\boldsymbol{J}}\dot{\boldsymbol{q}}) + \boldsymbol{Z}(\dot{\boldsymbol{\nu}}_c - \dot{\boldsymbol{Z}}^{\#}\dot{\boldsymbol{q}}) - \boldsymbol{M}^{-1}\boldsymbol{\tau}_{\text{ext}}. \tag{22}$$

Multiplying both sides of (22) by $\boldsymbol{Z}^{\#}$, and considering that $\dot{\boldsymbol{\nu}} = \dot{\boldsymbol{Z}}^{\#}\dot{\boldsymbol{q}} + \boldsymbol{Z}^{\#}\ddot{\boldsymbol{q}}$, the null-space closed-loop equation is obtained as

$$\dot{\boldsymbol{\nu}} = \dot{\boldsymbol{\nu}}_c - \boldsymbol{Z}^{\#}\boldsymbol{M}^{-1}\boldsymbol{\tau}_{\text{ext}}. \tag{23}$$

On the other hand, multiplying both sides of (22) by $\boldsymbol{J}$, (12) is recovered. Hence, the systems dynamics is fully described by the m task-space equations (12) and the $n-m$ null-space equations (23).

Notice that the null-space velocity vector $\boldsymbol{\nu}$ is, in general, nonintegrable [31], and thus, a null-space position error cannot be easily defined. However, similar to [32], a projected joint space error can be used to define the null-space command acceleration

$$\dot{\boldsymbol{\nu}}_c = \dot{\boldsymbol{\nu}}_d + \boldsymbol{\Lambda}_\nu^{-1}((\boldsymbol{\mu}_\nu + \boldsymbol{B}_\nu)\tilde{\boldsymbol{\nu}} + \boldsymbol{Z}^T\boldsymbol{K}_d\tilde{\boldsymbol{q}}) \tag{24}$$

with $\boldsymbol{K}_d, \boldsymbol{B}_\nu$ symmetric and positive-definite matrix, $\tilde{\boldsymbol{\nu}} = \boldsymbol{\nu}_d - \boldsymbol{\nu}$. The configuration-dependent quantities $\boldsymbol{\Lambda}_\nu = \boldsymbol{Z}^T\boldsymbol{M}\boldsymbol{Z}$ and $\boldsymbol{\mu}_\nu$ are, respectively, the inertia matrix and the Coriolis/centrifugal matrix in the null space (see Appendix A). The corresponding closed-loop equation is

$$\boldsymbol{\Lambda}_\nu\dot{\tilde{\boldsymbol{\nu}}} + (\boldsymbol{\mu}_\nu + \boldsymbol{B}_\nu)\tilde{\boldsymbol{\nu}} + \boldsymbol{Z}^T\boldsymbol{K}_d\tilde{\boldsymbol{q}} = \boldsymbol{Z}^T\boldsymbol{\tau}_{\text{ext}} \tag{25}$$

where $\boldsymbol{Z}^T\boldsymbol{\tau}_{\text{ext}}$ is the projection of the external torque on the null space. Equation (25) can be interpreted as an impedance equation defined in the null space, with inertia $\boldsymbol{\Lambda}_\nu$, damping $\boldsymbol{B}_\nu$, and projected elastic torque $\boldsymbol{Z}^T\boldsymbol{K}_d\tilde{\boldsymbol{q}}$.

D. Task-Space Control

In view of the task-space dynamics (12), it is clear that any interaction on the body of the manipulator may produce deviations from the desired task, depending on the choice of the command acceleration. To track a desired trajectory $\boldsymbol{x}_d(t)$, a common choice is that usually denoted as task-space resolved acceleration control [37]

$$\ddot{\boldsymbol{x}}_c = \ddot{\boldsymbol{x}}_d + \boldsymbol{K}_v\dot{\tilde{\boldsymbol{x}}} + \boldsymbol{K}_p\tilde{x} \tag{26}$$

with $\tilde{\boldsymbol{x}} = \boldsymbol{x}_d - \boldsymbol{x}$ and positive-definite matrices $\boldsymbol{K}_v$ and $\boldsymbol{K}_p$, which produces a linear closed-loop dynamics in the absence of interaction.

Another choice is that known as task-space passivity-based control, namely

$$\ddot{\boldsymbol{x}}_c = \ddot{\boldsymbol{x}}_d + \boldsymbol{P}\dot{\tilde{\boldsymbol{x}}} + \boldsymbol{\Lambda}_x^{-1}(\boldsymbol{\mu}_x + \boldsymbol{K})\boldsymbol{s} \tag{27}$$

where $\boldsymbol{\Lambda}_x$ and $\boldsymbol{\mu}_x$ are, respectively, the inertia matrix and the Coriolis/centrifugal matrix in the task space (see Appendix A). In (27), $\boldsymbol{s} = \dot{\tilde{\boldsymbol{x}}} + \boldsymbol{P}\tilde{\boldsymbol{x}}$, and $\boldsymbol{P}$ and $\boldsymbol{K}$ are positive-definite diagonal matrices. This control law preserves the passivity of the robot's dynamics.

A further choice is that known as task-space PD+ control, i.e.,

$$\ddot{\boldsymbol{x}}_c = \ddot{\boldsymbol{x}}_d + \boldsymbol{\Lambda}_x^{-1}((\boldsymbol{\mu}_x + \boldsymbol{D})\dot{\tilde{\boldsymbol{x}}} + \boldsymbol{K}\tilde{\boldsymbol{x}}) \tag{28}$$

with symmetric positive-definite matrices $\boldsymbol{K}$, $\boldsymbol{D}$. In this case, the closed-loop dynamics remains nonlinear as for passivity-based control.

Notice that in the task-space command accelerations (27) and (28), as well as, in the null-space command acceleration (24), the components $\boldsymbol{\mu}_x$ and $\boldsymbol{\mu}_\nu$ of Coriolis and centrifugal forces are reintroduced, after that they are completely compensated in the control torque (21), to ensure stability. An equivalent approach could be that of compensating in the control torque (21) only the components of the Coriolis and centrifugal torques corresponding to the cross terms $\boldsymbol{\mu}_{x\nu}$ and $\boldsymbol{\mu}_{\nu x}$ which couple the task-space and the null-space dynamics (see Appendix A), thus avoiding reintroducing $\boldsymbol{\mu}_x$ in (27) and (28) and $\boldsymbol{\mu}_\nu$ in (24). This may result in a more efficient implementation of the controller. Similar considerations can be made for the control laws proposed in the following sections.

It is worth remarking that the noncompensated interaction torques in the task-space dynamics (12) produce task-space errors that could be reduced by using high gains in the command accelerations (26)–(28). However, a more effective solution is that of estimating and compensating the external torques acting on the task variables. To this aim, two different approaches, based on suitable disturbance observers, are proposed in the following sections.

III. Task Error-Based Disturbance Observer

In this section, a disturbance observer based on the error introduced on the task space during external interaction is developed. The following propositions hold for constant $\boldsymbol{x}_d$ and $\boldsymbol{q}_d$.

Proposition 1: Let $\widehat{\boldsymbol{\tau}}$ denote the estimated external torque and $\tilde{\boldsymbol{\tau}} = \boldsymbol{\tau}_{\text{ext}} - \widehat{\boldsymbol{\tau}}$ denote the estimation error. Under the assumption of constant (or slowly time-varying) unknown external torque, the control law (21), with the joint space command acceleration (20) and the task-space command acceleration

$$\ddot{\boldsymbol{x}}_c = -\boldsymbol{P}\dot{\boldsymbol{x}} + \boldsymbol{\Lambda}_x^{-1}((\boldsymbol{\mu}_x + \boldsymbol{K})\boldsymbol{s} + \boldsymbol{J}^{\#T}\widehat{\boldsymbol{\tau}}) \tag{29}$$

with the disturbance observer

$$\dot{\widehat{\boldsymbol{\tau}}} = -\boldsymbol{\Gamma}_f^{-1}\boldsymbol{J}^{\#}\boldsymbol{s} \tag{30}$$

together with the null-space command acceleration

$$\dot{\boldsymbol{\nu}}_c = -\boldsymbol{\Lambda}_\nu^{-1}((\boldsymbol{\mu}_\nu + \boldsymbol{B}_\nu)\boldsymbol{\nu} - \boldsymbol{Z}^T\boldsymbol{K}_d\tilde{\boldsymbol{q}}) \tag{31}$$

guarantees that $\tilde{\boldsymbol{x}}$, $\dot{\boldsymbol{x}}$, and $\boldsymbol{\nu}$ go to zero asymptotically, while a compliant behavior is imposed in the null space of the main

task. Moreover, $\widehat{\boldsymbol{\tau}}$ remains bounded, and the closed-loop system is stable. In the aforementioned controller, $\boldsymbol{s} = -\dot{\boldsymbol{x}} + \boldsymbol{P}\tilde{\boldsymbol{x}}$, $\boldsymbol{K}_d$ is a diagonal and positive-definite matrix and $\boldsymbol{B}_\nu$ and $\boldsymbol{\Gamma}_f$ are positive-definite constant matrices.

The command acceleration (29) coincides with passivity-based control (27) with the addition of a term to compensate the effect of the external torque on the task space. By using the command acceleration (29) together with (21), (20), and (31), the control torque can be written as

$$\boldsymbol{\tau} = \boldsymbol{\tau}_{\text{task}} + \boldsymbol{\tau}_{\text{null}} + \boldsymbol{C}(\boldsymbol{q}, \dot{\boldsymbol{q}})\dot{\boldsymbol{q}} + \boldsymbol{g}(\boldsymbol{q}) \tag{32}$$

with

$$\boldsymbol{\tau}_{\text{task}} = \boldsymbol{J}^T(\boldsymbol{\Lambda}_x(-\boldsymbol{P}\dot{\boldsymbol{x}} - \dot{\boldsymbol{J}}\dot{\boldsymbol{q}}) + (\boldsymbol{\mu}_x + \boldsymbol{K})\boldsymbol{s} + \boldsymbol{J}^{\#T}\widehat{\boldsymbol{\tau}}) \tag{33}$$

$$\boldsymbol{\tau}_{\text{null}} = -\boldsymbol{Z}^{\#T}(\boldsymbol{\Lambda}_\nu \dot{\boldsymbol{Z}}^{\#}\dot{\boldsymbol{q}} + (\boldsymbol{\mu}_\nu + \boldsymbol{B}_\nu)\boldsymbol{\nu} + \boldsymbol{Z}^T\boldsymbol{K}_d\tilde{\boldsymbol{q}}). \tag{34}$$

These equations reveal that the control law is a combination of three different parts which are responsible for task-space control ($\boldsymbol{\tau}_{\text{task}}$), null-space control ($\boldsymbol{\tau}_{\text{null}}$), and Coriolis/gravity compensation, respectively.

The stability proof of the overall control algorithm is based on the concept of conditional stability, first used in [32] to prove the stability of compliance control of redundant robots. For the purpose of this paper, the following theorem, which allows us to prove asymptotic stability with semidefinite Lyapunov functions, is exploited.

Theorem 1 [38]: Let $\boldsymbol{z} = \boldsymbol{0}$ be an equilibrium point for $\dot{\boldsymbol{z}} = \boldsymbol{f}(\boldsymbol{z})$. If in a neighborhood $\boldsymbol{\Omega}$ of the origin there exists a function $V \in C^1$ such that

1) $V(\boldsymbol{z}) \geq 0$ for all $\boldsymbol{z} \in \boldsymbol{\Omega}$ and $V(\boldsymbol{0}) = \boldsymbol{0}$;
2) $\dot{V}(\boldsymbol{z}) \leq 0$ for all $\boldsymbol{z} \in \boldsymbol{\Omega}$;
3) on the largest positively invariant set $\mathcal{L}$ contained in $\{\boldsymbol{z} \in \boldsymbol{\Omega} | \dot{V}(\boldsymbol{z}) = 0\}$, the system is asymptotically stable (i.e., it is asymptotically stable conditionally to $\mathcal{L}$);

Then, the origin is asymptotically stable.

Proof of Proposition 1: The control law (21) with the joint space command acceleration (20) gives (12) and (23). Hence, by replacing the command acceleration (29) into (12), the closed-loop dynamics in the task space is achieved as

$$-\ddot{\boldsymbol{x}} - \boldsymbol{P}\dot{\boldsymbol{x}} + \boldsymbol{\Lambda}_x^{-1}((\boldsymbol{\mu}_x + \boldsymbol{K})\boldsymbol{s} + \boldsymbol{J}^{\#T}\widehat{\boldsymbol{\tau}}) = \boldsymbol{J}\boldsymbol{M}^{-1}\boldsymbol{\tau}_{\text{ext}} \tag{35}$$

which further reduces to

$$\boldsymbol{\Lambda}_x\dot{\boldsymbol{s}} + (\boldsymbol{\mu}_x + \boldsymbol{K})\boldsymbol{s} = \boldsymbol{J}^{\#T}\tilde{\boldsymbol{\tau}} \tag{36}$$

$$\boldsymbol{J}^{\#T}\tilde{\boldsymbol{\tau}} = \tilde{\boldsymbol{F}} = \boldsymbol{F}_{\text{ext}} - \widehat{\boldsymbol{F}} \tag{37}$$

where $\widehat{\boldsymbol{F}} = \boldsymbol{J}^{\#T}\widehat{\boldsymbol{\tau}}$ is the estimation of $\boldsymbol{F}_{\text{ext}} = \boldsymbol{J}^{\#T}\boldsymbol{\tau}_{\text{ext}}$. Moreover, by replacing the null-space acceleration (31) in (23), the closed-loop dynamics (25) is achieved in the null space.

In summary, the closed-loop equations of the system with state vector $\boldsymbol{z} = (\tilde{\boldsymbol{q}}, \tilde{\boldsymbol{x}}, \boldsymbol{s}, \boldsymbol{\nu}, \tilde{\boldsymbol{\tau}})$ are given by

$$\begin{aligned}
&\dot{\boldsymbol{q}} = \boldsymbol{J}^{\#}\dot{\boldsymbol{x}} + \boldsymbol{Z}\boldsymbol{\nu}\\
&\boldsymbol{\Lambda}_x\dot{\boldsymbol{s}} + (\boldsymbol{\mu}_x + \boldsymbol{K})\boldsymbol{s} = \boldsymbol{J}^{\#T}\tilde{\boldsymbol{\tau}}\\
&\boldsymbol{\Lambda}_\nu\dot{\boldsymbol{\nu}} + (\boldsymbol{\mu}_\nu + \boldsymbol{B}_\nu)\boldsymbol{\nu} + \boldsymbol{Z}^T\boldsymbol{K}_d\tilde{\boldsymbol{q}} = \boldsymbol{Z}^T\boldsymbol{\tau}_{\text{ext}}\\
&\dot{\widehat{\boldsymbol{\tau}}} = -\boldsymbol{\Gamma}_f^{-1}\boldsymbol{J}^{\#}\boldsymbol{s}\\
&\boldsymbol{s} = -\dot{\boldsymbol{x}} + \boldsymbol{P}\tilde{\boldsymbol{x}}.
\end{aligned} \tag{38}$$

Let us consider the function

$$V(\tilde{\boldsymbol{q}}, \tilde{\boldsymbol{x}}, \boldsymbol{s}, \tilde{\boldsymbol{\tau}}) = \tilde{\boldsymbol{x}}^T\boldsymbol{P}\boldsymbol{K}\tilde{\boldsymbol{x}} + \frac{1}{2}\boldsymbol{s}^T\boldsymbol{\Lambda}_x\boldsymbol{s} + \frac{1}{2}\tilde{\boldsymbol{\tau}}^T\boldsymbol{\Gamma}_f\tilde{\boldsymbol{\tau}} \tag{39}$$

which is nonnegative because $\boldsymbol{P}$ and $\boldsymbol{K}$ are positive-definite diagonal matrices, and $\boldsymbol{\Lambda}_x$ and $\boldsymbol{\Gamma}_f$ are symmetric and positive-definite matrices. The quadratic form V is only positive semidefinite because it does not depend on the full state $\boldsymbol{z}$. The time derivative of (39) along the system trajectories is

$$\dot{V} = -2\tilde{\boldsymbol{x}}^T\boldsymbol{P}\boldsymbol{K}\dot{\boldsymbol{x}} + \boldsymbol{s}^T\boldsymbol{\Lambda}_x\dot{\boldsymbol{s}} + \frac{1}{2}\boldsymbol{s}^T\dot{\boldsymbol{\Lambda}}_x\boldsymbol{s} + \dot{\tilde{\boldsymbol{\tau}}}^T\boldsymbol{\Gamma}_f\tilde{\boldsymbol{\tau}}. \tag{40}$$

Using (30) and (36) yields the equation

$$\begin{aligned}
\dot{V} = &-2\tilde{\boldsymbol{x}}^T\boldsymbol{P}\boldsymbol{K}\dot{\boldsymbol{x}} + \boldsymbol{s}^T(\boldsymbol{J}^{\#T}\tilde{\boldsymbol{\tau}} - (\boldsymbol{\mu}_x + \boldsymbol{K})\boldsymbol{s})\\
&+ \frac{1}{2}\boldsymbol{s}^T\dot{\boldsymbol{\Lambda}}_x\boldsymbol{s} - \boldsymbol{s}^T\boldsymbol{J}^{\#T}\tilde{\boldsymbol{\tau}}
\end{aligned} \tag{41}$$

that, by considering the skew-symmetry of $\dot{\boldsymbol{\Lambda}}_x - 2\boldsymbol{\mu}_x$, can be rewritten as

$$\dot{V} = -2\tilde{\boldsymbol{x}}^T\boldsymbol{P}\boldsymbol{K}\dot{\boldsymbol{x}} - \boldsymbol{s}^T\boldsymbol{K}\boldsymbol{s}. \tag{42}$$

Moreover, by replacing $\boldsymbol{s} = -\dot{\boldsymbol{x}} + \boldsymbol{P}\tilde{\boldsymbol{x}}$ in (42), we obtain

$$\dot{V} = -\dot{\boldsymbol{x}}^T\boldsymbol{K}\dot{\boldsymbol{x}} - \tilde{\boldsymbol{x}}^T\boldsymbol{P}\boldsymbol{K}\boldsymbol{P}\tilde{\boldsymbol{x}} \leq 0. \tag{43}$$

Function V satisfies the hypothesis of Theorem 1. In order to show the asymptotic stability of the whole system, the asymptotic stability of the system conditionally to subset $\mathcal{L} = \{\tilde{\boldsymbol{q}}, \boldsymbol{\nu}, \tilde{\boldsymbol{\tau}}, \tilde{\boldsymbol{x}} = \boldsymbol{0}, \boldsymbol{s} = \boldsymbol{0}\}$ must be shown. This can be proven by considering the Lyapunov function candidate

$$V_{\mathcal{L}} = \frac{1}{2}\boldsymbol{\nu}^T\boldsymbol{\Lambda}_\nu(\boldsymbol{q})\boldsymbol{\nu} + \frac{1}{2}\tilde{\boldsymbol{q}}^T\boldsymbol{K}_d\tilde{\boldsymbol{q}} + \frac{1}{2}\tilde{\boldsymbol{\tau}}^T\boldsymbol{\Gamma}_f\tilde{\boldsymbol{\tau}} \tag{44}$$

which is positive definite in $\mathcal{L}$ and positive semidefinite in the whole state space, where $\boldsymbol{\Lambda}_\nu(\boldsymbol{q})$ and $\boldsymbol{K}_d$ are symmetric and positive-definite matrices. The time derivative of $V_{\mathcal{L}}$ can be computed as

$$\begin{aligned}
\dot{V}_{\mathcal{L}} = &-\boldsymbol{\nu}^T\boldsymbol{B}_\nu\boldsymbol{\nu} - \boldsymbol{\nu}^T\boldsymbol{Z}^T\boldsymbol{K}_d\tilde{\boldsymbol{q}} + \boldsymbol{\nu}^T\boldsymbol{Z}^T\boldsymbol{\tau}_{\text{ext}}\\
&- \dot{\boldsymbol{q}}^T\boldsymbol{K}_d\tilde{\boldsymbol{q}} + \dot{\tilde{\boldsymbol{\tau}}}^T\boldsymbol{\Gamma}_f\tilde{\boldsymbol{\tau}}.
\end{aligned} \tag{45}$$

Note that in the set $\mathcal{L}$, $\boldsymbol{s} = \boldsymbol{0}$, and the last term on the right-hand side of (45) is null in view of (30). Furthermore, in this set, (19) reduces to $\dot{\boldsymbol{q}} = \boldsymbol{Z}\boldsymbol{\nu}$.

Consider first the case where $\boldsymbol{Z}^T\boldsymbol{\tau}_{\text{ext}} = \boldsymbol{0}$ and the desired configuration $\boldsymbol{q}_d$ is chosen so that $\boldsymbol{x}_d = \boldsymbol{x}(\boldsymbol{q}_d)$, where $\boldsymbol{x}(\cdot)$ is the robot direct kinematic equation. In this case, (45) reduces to

$$\dot{V}_{\mathcal{L}} = -\boldsymbol{\nu}^T\boldsymbol{B}_\nu\boldsymbol{\nu} \leq 0. \tag{46}$$

The asymptotic stability in the set $\mathcal{L}$ can be proven using the La Salle's invariance principle. In detail, the state converges to the largest invariant set with $\boldsymbol{\nu} = \boldsymbol{0}$ in set $\mathcal{L}$. From the closed-loop system, this invariant set is given by $\{\boldsymbol{s} = \boldsymbol{0}, \tilde{\boldsymbol{x}} = \boldsymbol{0}, \boldsymbol{\nu} = \boldsymbol{0}, \boldsymbol{J}^{\#T}\tilde{\boldsymbol{\tau}} = \boldsymbol{0}, \boldsymbol{Z}^T\boldsymbol{K}_d\tilde{\boldsymbol{q}} = \boldsymbol{0}\}$. Remarkably, as shown in Appendix B, the solution of equation $\boldsymbol{Z}^T\boldsymbol{K}_d\tilde{\boldsymbol{q}} = \boldsymbol{0}$, with the constraint $\boldsymbol{x}(\boldsymbol{q}) = \boldsymbol{x}_d$, is $\tilde{\boldsymbol{q}} = \boldsymbol{0}$ and is an isolated point. Thus, the system is asymptotically stable conditionally to $\mathcal{L}$. By virtue of Theorem 1, the system asymptotically converges to $\{\boldsymbol{s} = \boldsymbol{0}, \boldsymbol{x} = \boldsymbol{x}_d, \boldsymbol{\nu} = \boldsymbol{0}, \boldsymbol{J}^{\#T}\tilde{\boldsymbol{\tau}} = \boldsymbol{0}, \boldsymbol{q} = \boldsymbol{q}_d\}$.

In the case of a non-null and constant external torque $\boldsymbol{\tau}_{\text{ext}}$, or in the case $\boldsymbol{x}(\boldsymbol{q}_d) \neq \boldsymbol{x}_d$, the asymptotic stability is still preserved, but the system reaches a different equilibrium $\{\boldsymbol{s} = \boldsymbol{0}, \boldsymbol{x} = \boldsymbol{x}_d, \boldsymbol{\nu} = \boldsymbol{0}, \boldsymbol{J}^{\#T}\tilde{\boldsymbol{\tau}} = \boldsymbol{0}, \boldsymbol{q} = \boldsymbol{q}^*\}$, where $\boldsymbol{q}^*$ belongs to the set of solutions of equation

$$\boldsymbol{Z}^T(\boldsymbol{K}_d\tilde{\boldsymbol{q}} - \boldsymbol{\tau}_{\text{ext}}) = \boldsymbol{0} \tag{47}$$

which locally minimize the quadratic function $\|\boldsymbol{K}_d\tilde{\boldsymbol{q}} - \boldsymbol{\tau}_{\text{ext}}\|^2$, with the constraint $\boldsymbol{x}(\boldsymbol{q}) = \boldsymbol{x}_d$. □

The controller–observer law of Proposition 1 can be modified according to Proposition 2 where the command acceleration is based on the PD+ controller written in the task space (28).

Proposition 2: The task-space command acceleration and disturbance observer in Proposition 1 can be replaced by

$$\ddot{\boldsymbol{x}}_c = \boldsymbol{\Lambda}_x^{-1}(-(\boldsymbol{\mu}_x + \boldsymbol{D})\dot{\boldsymbol{x}} + \boldsymbol{K}\tilde{\boldsymbol{x}} + \boldsymbol{J}^{\#T}\widehat{\boldsymbol{\tau}}) \tag{48}$$

and disturbance observer

$$\dot{\widehat{\boldsymbol{\tau}}} = -\boldsymbol{\Gamma}_f^{-1}\boldsymbol{J}^{\#}(-\dot{\boldsymbol{x}} + \gamma\boldsymbol{f}(\tilde{\boldsymbol{x}})) \tag{49}$$

$$\boldsymbol{f}(\tilde{\boldsymbol{x}}) = \frac{1}{1 + \|\tilde{\boldsymbol{x}}\|}\tilde{\boldsymbol{x}} \tag{50}$$

where γ is a properly chosen constant positive gain. The stability of whole system, the convergence of $\tilde{\boldsymbol{x}}$, $\dot{\boldsymbol{x}}$, and $\boldsymbol{\nu}$ to zero, and the compliant behavior in the null space of the main task are preserved.

Sketch of proof: The closed-loop equation in the task space can be computed from (48) and (12) as

$$-\boldsymbol{\Lambda}_x\ddot{\boldsymbol{x}} - (\boldsymbol{\mu}_x + \boldsymbol{D})\dot{\boldsymbol{x}} + \boldsymbol{K}\tilde{\boldsymbol{x}} = \boldsymbol{J}^{\#T}\tilde{\boldsymbol{\tau}}. \tag{51}$$

The left side of this equation is equivalent to the closed-loop system of the well-known PD+ control law [39] designed in the task space, that can be obtained by replacing (48) in (20) and (21), i.e.,

$$\boldsymbol{\tau}_{\text{task}} = \boldsymbol{J}^T(-\boldsymbol{\Lambda}_x\dot{\boldsymbol{J}}\dot{\boldsymbol{q}} - (\boldsymbol{\mu}_x + \boldsymbol{D})\dot{\boldsymbol{x}} + \boldsymbol{K}\tilde{\boldsymbol{x}}) + \boldsymbol{J}^T\boldsymbol{J}^{\#T}\widehat{\boldsymbol{\tau}}\,. \tag{52}$$

The null-space contribution to the control torque is the same as in (34) and the corresponding closed-loop equation in the null space is that in (25).

The hypothesis of Theorem 1 can be satisfied with a more elaborate positive-semidefinite Lyapunov function candidate, inspired to the strict Lyapunov function for PD+ control introduced in [40]

$$V(\tilde{\boldsymbol{q}}, \tilde{\boldsymbol{x}}, \dot{\boldsymbol{x}}, \tilde{\boldsymbol{\tau}}) = \frac{1}{2}\dot{\boldsymbol{x}}^T\boldsymbol{\Lambda}_{\boldsymbol{x}}\dot{\boldsymbol{x}} + \frac{1}{2}\tilde{\boldsymbol{x}}^T\boldsymbol{K}\tilde{\boldsymbol{x}} - \gamma\boldsymbol{f}(\tilde{\boldsymbol{x}})^T\boldsymbol{\Lambda}_x\dot{\boldsymbol{x}} + \frac{1}{2}\tilde{\boldsymbol{\tau}}^T\boldsymbol{\Gamma}_f\tilde{\boldsymbol{\tau}}. \tag{53}$$

The time derivative of V along system trajectory (49) and (51) is negative semidefinite under some special bound on γ (see [40]). The asymptotic stability conditionally to $\mathcal{L}$ and the asymptotic stability of the whole system can be shown with a proof similar to that in Proposition 1. □

Remark 1: In Proposition 1 and 2, the non-minimal form command acceleration

$$\ddot{\boldsymbol{q}}_c = \boldsymbol{J}^{\#}(\ddot{\boldsymbol{x}}_c - \dot{\boldsymbol{J}}\dot{\boldsymbol{q}}) + \boldsymbol{N}_{\#}(\boldsymbol{M}^{-1}(-\boldsymbol{B}_d\dot{\boldsymbol{q}} + \boldsymbol{K}_d\tilde{\boldsymbol{q}})) \tag{54}$$

can be used instead of (20). Despite this choice seeming to be more intuitive, the stability proof is not easy, since the parameterization of the null-space position and velocity errors is non-minimal.

Remark 2: While the force estimation error $\tilde{\boldsymbol{F}} = \boldsymbol{J}^{\#T}\tilde{\boldsymbol{\tau}}$ goes to zero, the torque estimation error $\tilde{\boldsymbol{\tau}}$ converges to zero only for nonredundant robots. Hence, the disturbance observer provides an estimate of the equivalent force reflected at the end effector. In principle, (30) could be replaced by a simpler linear integral action on the variable $\boldsymbol{s}$, i.e., ($\dot{\widehat{\boldsymbol{F}}} = -\boldsymbol{\Gamma}_f^{-T}\boldsymbol{s}$) to directly compute $\widehat{\boldsymbol{F}}$. With similar arguments, it is possible to prove asymptotic convergence to zero of the task-space error and of the force estimation error $\tilde{\boldsymbol{F}}$. However, this requires $\boldsymbol{F}_{\text{ext}}$, which is the reflection of $\boldsymbol{\tau}_{\text{ext}}$ on the task space, to be a slowly time-varying vector. In the applications considered here, the interaction occurs on the robot body and not on the end effector. This implies that the reflected force $\boldsymbol{F}_{\text{ext}} = \boldsymbol{J}^{\#T}\boldsymbol{\tau}_{\text{ext}}$ on the task space is, in general, highly dependent on the joint configuration, which changes during the interaction so that this assumption cannot be held.

IV. Momentum-Based Observer

Another method for perfect task execution during interaction is proposed here, relying on the momentum-based observer introduced in [3] and [6]. The basic concepts are the generalized momentum $\boldsymbol{p}(t) = \boldsymbol{M}(\boldsymbol{q})\dot{\boldsymbol{q}}$, and the n-dimensional residual vector $\boldsymbol{r}$ is defined as

$$\boldsymbol{r}(t) = \boldsymbol{K}_I\left[\boldsymbol{p}(t) - \int_0^t(\boldsymbol{\tau} + \boldsymbol{C}^T(\boldsymbol{q}, \dot{\boldsymbol{q}})\dot{\boldsymbol{q}} - \boldsymbol{g}(\boldsymbol{q}) + \boldsymbol{r}(\sigma))d\sigma\right] \tag{55}$$

with $\boldsymbol{r}(0) = \boldsymbol{0}$, $\boldsymbol{K}_I$ a diagonal positive matrix, and $\boldsymbol{p}(0) = \boldsymbol{0}$. These quantities can be computed using measured signal $\boldsymbol{q}$, $\dot{\boldsymbol{q}}$ and the commanded torque $\boldsymbol{\tau}$. It can be shown that the dynamics of $\boldsymbol{r}$ are

$$\dot{\boldsymbol{r}} = -\boldsymbol{K}_I\boldsymbol{r} - \boldsymbol{K}_I\boldsymbol{\tau}_{\text{ext}}. \tag{56}$$

Thus, the residual vector is a filtered version of the real external torque, i.e.,

$$\boldsymbol{r}(t) \approx -\boldsymbol{\tau}_{\text{ext}}. \tag{57}$$

In the absence of interaction, assuming no noise and unmodeled disturbances, $\boldsymbol{r}(t) = \boldsymbol{0}$. As soon as collision occurs, the components of $\boldsymbol{r}$ will rise exponentially and will reach the value of $-\boldsymbol{\tau}_{\text{ext}}$. Therefore, the idea is that of using the residual vector as an estimate of the external torque in the task-space control law as detailed in Proposition 3.

Proposition 3: In the presence of constant (or slowly time-varying) unknown external torque, for positive-definite matrices $\boldsymbol{K}_v$ and $\boldsymbol{K}_p$, the control law given by (20), (21), and the task-space command acceleration

$$\ddot{\boldsymbol{x}}_c = -\boldsymbol{K}_v\dot{\boldsymbol{x}} + \boldsymbol{K}_p\tilde{\boldsymbol{x}} - \boldsymbol{\Lambda}_x^{-1}\boldsymbol{J}^{\#T}\boldsymbol{r} \tag{58}$$

together with null-space command acceleration (31) and residual dynamics (55), guarantees that $\tilde{\boldsymbol{x}}, \dot{\boldsymbol{x}}, \boldsymbol{\nu}$, and estimation error $\tilde{\boldsymbol{r}} = \boldsymbol{r} + \boldsymbol{\tau}_{\text{ext}}$, go to zero asymptotically, while a desired compliant behavior is imposed in the null space of the main task.

Proof of Proposition 3: From (12) and (56), the closed-loop error dynamics are

$$-\ddot{\boldsymbol{x}} - \boldsymbol{K}_v\dot{\tilde{\boldsymbol{x}}} + \boldsymbol{K}_p\tilde{\boldsymbol{x}} = \boldsymbol{\Lambda}_x^{-1}\boldsymbol{J}^{\#T}\tilde{\boldsymbol{r}} \tag{59}$$

$$\dot{\tilde{\boldsymbol{r}}} + \boldsymbol{K}_I\tilde{\boldsymbol{r}} = \dot{\boldsymbol{\tau}}_{\text{ext}}. \tag{60}$$

The closed-loop dynamics for the null space are the same as in (25).

The stability analysis is based on a lemma from the stability of perturbed system ([41, Lemma 9.1, p. 341]). For constant (or slowly time-varying) unknown external torque, the closed-loop equations (59) and (60) can be considered as a perturbed linear system

$$\dot{\boldsymbol{z}} = \boldsymbol{A}\boldsymbol{z} + \boldsymbol{g}(t, \boldsymbol{z}) \tag{61}$$

with state vector $\boldsymbol{z} = (\tilde{\boldsymbol{x}}, \dot{\boldsymbol{x}}, \tilde{\boldsymbol{r}})$, and the perturbation $\boldsymbol{g}(t, \boldsymbol{z})$. By properly choosing $\boldsymbol{K}_v$ and $\boldsymbol{K}_p$, the equilibrium point $\boldsymbol{z} = \boldsymbol{0}$ is exponentially stable for the linear system $\dot{\boldsymbol{z}} = \boldsymbol{A}\boldsymbol{z}$. Thus, the quadratic function

$$V(\boldsymbol{z}) = \frac{1}{2}\dot{\boldsymbol{x}}^T\dot{\boldsymbol{x}} + \frac{1}{2}\tilde{\boldsymbol{x}}^T\boldsymbol{K}_p\tilde{\boldsymbol{x}} + \frac{1}{2}\tilde{\boldsymbol{r}}^T\tilde{\boldsymbol{r}} \tag{62}$$

can be defined which satisfies the following conditions:

$$c_1\|\boldsymbol{z}\|^2 \le V(\boldsymbol{z}) \le c_2\|\boldsymbol{z}\|^2 \tag{63}$$

$$\dot{V}(\boldsymbol{z}) = \frac{\partial V}{\partial \boldsymbol{z}}\boldsymbol{A}\boldsymbol{z} \le -c_3\|\boldsymbol{z}\|^2 \tag{64}$$

$$\left\| \frac{\partial V}{\partial \boldsymbol{z}} \right\| \le c_4 \left\| \boldsymbol{z} \right\| \tag{65}$$

for some positive constants c_1, c_2, c_3, and c_4. Notice that (62) is positive semidefinite for the whole system, but it is positive definite for the linear part of (61).

The perturbation term satisfies the linear growth bound

$$\|\boldsymbol{J}\boldsymbol{M}^{-1}\tilde{\boldsymbol{r}}\| \le \gamma\|\boldsymbol{z}\| \tag{66}$$

for non-negative γ, were $\boldsymbol{J}$ and $\boldsymbol{M}^{-1}$ are bounded matrices in case of revolute joints and nonsingular configurations. The time derivative of $V(\boldsymbol{z})$ along the trajectory of perturbed system is given by

$$\dot{V}(\boldsymbol{z}) = \frac{\partial V}{\partial \boldsymbol{z}}\boldsymbol{A}\boldsymbol{z} + \frac{\partial V}{\partial \boldsymbol{z}}\boldsymbol{g}(t, \boldsymbol{z}). \tag{67}$$

Using (63)–(65), we obtain

$$\begin{aligned}\dot{V}(\boldsymbol{z}) &\le -c_3\|\boldsymbol{z}\|^2 + \|\frac{\partial V}{\partial \boldsymbol{z}}\| \ \|\boldsymbol{g}(t, \boldsymbol{z})\| \\ &\le -c_3\|\boldsymbol{z}\|^2 + c_4\gamma\|\boldsymbol{z}\|^2 \\ &\le -(c_3 - c_4\gamma)\|\boldsymbol{z}\|^2. \end{aligned} \tag{68}$$

If γ is small enough to satisfy the bound $\gamma < c_3/c_4$, then the system is exponentially stable in the task space. In order to show the asymptotic stability of the whole system, using Theorem 1, the asymptotic stability of the system conditionally to $\mathcal{L} = \{\boldsymbol{z} | \dot{V}(\boldsymbol{z}) = 0\}$ must be shown. Notice that the time derivative of (62) along the system trajectories is

$$\dot{V}(\boldsymbol{z}) = -\dot{\boldsymbol{x}}^T\boldsymbol{K}_v\dot{\boldsymbol{x}} - \dot{\boldsymbol{x}}\boldsymbol{J}\boldsymbol{M}^{-1}\tilde{\boldsymbol{r}} - \tilde{\boldsymbol{r}}^T\boldsymbol{K}_I\tilde{\boldsymbol{r}} \tag{69}$$

and thus, the subset $\mathcal{L}$ is given by $\mathcal{L} = \{\tilde{\boldsymbol{q}}, \boldsymbol{\nu}, \tilde{\boldsymbol{x}} = \boldsymbol{0}, \dot{\boldsymbol{x}} = \boldsymbol{0}, \tilde{\boldsymbol{r}} = \boldsymbol{0}\}$, in view of (68). The Lyapunov function candidate

$$V_{\mathcal{L}} = \frac{1}{2}\boldsymbol{\nu}^T\boldsymbol{\Lambda}_\nu(\boldsymbol{q})\boldsymbol{\nu} + \frac{1}{2}\tilde{\boldsymbol{q}}^T\boldsymbol{K}_d\tilde{\boldsymbol{q}} \tag{70}$$

is defined on this set. From here, the same procedure used in the proof of Proposition 1 is adopted and asymptotic stability of the equilibrium point $\{\boldsymbol{x} = \boldsymbol{x}_d, \dot{\boldsymbol{x}} = \boldsymbol{0}, \boldsymbol{\nu} = \boldsymbol{0}, \tilde{\boldsymbol{r}} = \boldsymbol{0}, \boldsymbol{q} = \boldsymbol{q}^*\}$ is shown similarly. □

Remark 3: Despite the task-space command, (58) is simple and intuitive, experimental tests show that the behavior of the controlled system in the task space is greatly dependent on the joint configuration and can also have large task-space errors during fast interaction. The reason is that the residual torque error at the right-hand side of (59) is multiplied by the configuration-dependent matrix $\boldsymbol{\Lambda}_x^{-1}$. An alternative control law can be adopted, by using the PD+ controller

$$\ddot{\boldsymbol{x}}_c = \boldsymbol{\Lambda}_x^{-1}(-(\boldsymbol{\mu}_x + \boldsymbol{D})\dot{\boldsymbol{x}} + \boldsymbol{K}\tilde{\boldsymbol{x}} + \boldsymbol{J}^{\#T}\boldsymbol{r}) \tag{71}$$

leading to the closed-loop equation

$$-\boldsymbol{\Lambda}_x\ddot{\boldsymbol{x}} - (\boldsymbol{\mu}_x + \boldsymbol{D})\dot{\boldsymbol{x}} + \boldsymbol{K}\tilde{\boldsymbol{x}} = \boldsymbol{J}^{\#T}\tilde{\boldsymbol{r}} \tag{72}$$

which preserves the robot natural dynamics. The stability of the system can be shown by modifying the proof of Proposition 3 as in the proof of Proposition 2.

V. Experimental Evaluation

The proposed approaches are verified experimentally on a 7-DOF KUKA LWR4 lightweight arm ($n = 7$). Control algorithms are executed through fast research interface library [42] on a remote PC with the Ubunto operating system. The remote computer is connected to a KUKA robot controller unit through UDP socket with a sampling rate of 2 ms.

The experiments are performed for three cases: with no observer, with task error-based observer, and with momentum-based observer. In all the cases, the position of the end effector is assumed as the main task ($m = 3$). Therefore, the robot has 4 degrees of redundancy ($r = 4$).

To obtain the null-space projection matrix $\boldsymbol{Z}$, first the Jacobian matrix is written in partitioned form $\boldsymbol{J} = [\boldsymbol{J}_m \quad \boldsymbol{J}_r]$ such that $\boldsymbol{J}_m$ be invertible (see, e.g., [43]). The null-space base matrix is calculated by $\boldsymbol{Z} = [\boldsymbol{J}_r^T\boldsymbol{J}_m^{-T} \quad \boldsymbol{I}]^T$.

In the following, two different sets of experiments are considered. In all the experiments, the control laws (20) and (21), with dynamically consistent generalized inverse used, while different command acceleration are tested.

A. Experiment 1

In the first set of experiments, a constant configuration $\boldsymbol{q}_d = [\pi/4, -\pi/6, 0, -\pi/1.8, \pi/6, -\pi/4, 0]$ is considered, corresponding to the constant desired position of the end effector in the task space $\boldsymbol{x}_d = [-0.242, -0.133, 0.968]^T$.

The interaction occurs with an elastic ball of 1200 N/m approximate stiffness at a point of the robot arm close to the fourth joint. While the end effector is commanded to be in the desired position, the sphere comes in contact with the robot, stops for 10 s, and, finally, goes back far from the robot. In order to have

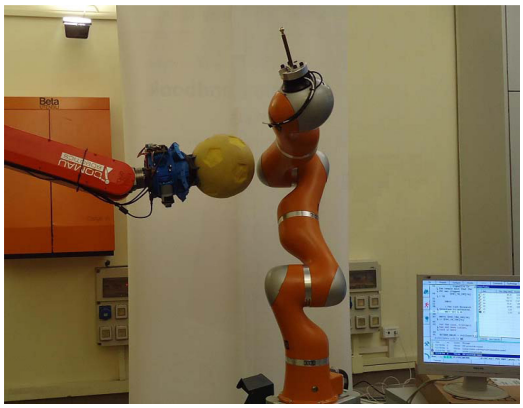

Fig. 2. Experiment 1: Elastic ball in interaction with a KUKA LWR4 arm.

the same scenario in all the experiments and guarantee repeatability, the ball is moved by a position-controlled industrial robot with constant speed of 4.5 cm/s along a straight line. A snapshot of the experimental setup is depicted in Fig. 2.

Case I—Interaction Control With No External Interaction Observer: The command acceleration given by (26) and (31) are considered, with the gains $\boldsymbol{K}_p = 2000$, $\boldsymbol{K}_v = 90$, $\boldsymbol{B}_\nu = 0.4\boldsymbol{I}$, and $\boldsymbol{K}_d = \text{diag}[10, 8, 8, 8, 8, 8, 8]$.

The corresponding main task error and the estimated external torques, obtained by the torque sensors available on LWR4 robot, together with the joints position, are shown in Fig. 3. The time interval when interaction occurs is identified by the two vertical lines. It can be observed that the task-space error components are zero initially, but after the collision with the sphere, they increase and reach constant values when the sphere stops. When the sphere is retreated and contact is lost, the task error components become small but non-null, due to the presence of non-negligible joint friction.

From the time histories of the joint variables, in Fig. 3, it can be argued that, during the interaction, the configuration of the robot changes and the redundancy allows the manipulator to comply with the external forces. As soon as the contact is lost, the robot comes back to its desired configuration. The behavior of the arm in the null space can be set by properly choosing the control gains.

The scenario is repeated again by using the PD+ task-space command acceleration (28) with $\boldsymbol{K} = 2000\boldsymbol{I}, \boldsymbol{D} = 90\boldsymbol{I}$. The task-space error for this case has been reported in Fig. 4. It can be seen that the error in task space is significantly lower than in the previous case. However, the error remains non-null, especially during the interaction. The corresponding estimated external torque and joints position do not change considerably and are not shown for brevity.

Case II—Interaction Control With the Task Error-Based Disturbance Observer: The previous experiment is repeated by using the command acceleration (29) with disturbance observer (30). The parameters of the controller are tuned as $\boldsymbol{P} = 25\boldsymbol{I}$, $\boldsymbol{K} = 80\boldsymbol{I}$, and $\boldsymbol{\Gamma}_f = 0.125\boldsymbol{I}$, and the null-space impedance matrices are selected as in the previous case.

The performance of the controller is shown in Fig. 5. Even though the external torque $\boldsymbol{\tau}_{\text{ext}}$ is not constant during the first

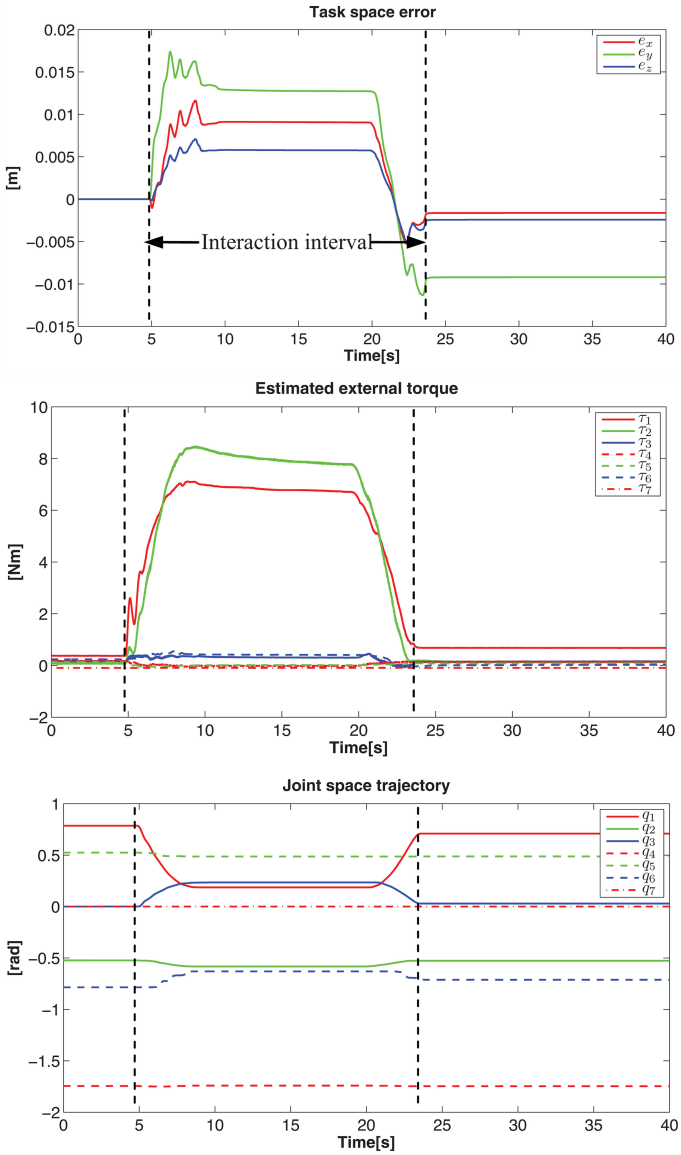

Fig. 3. Experiment 1: Task errors, external torques estimation evaluated from torque sensors and joint space trajectory, with no observer, using (26).

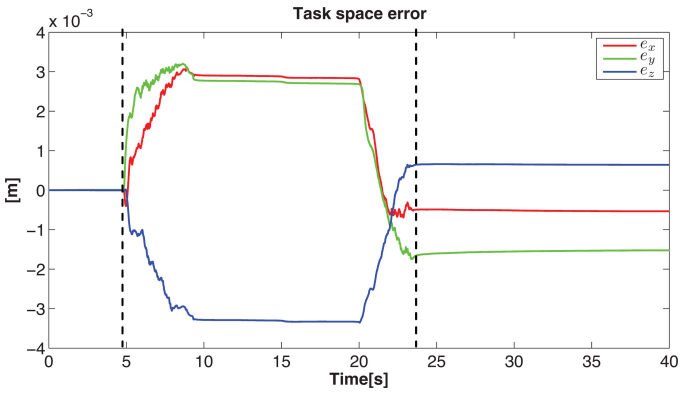

Fig. 4. Experiment 1: Task errors with no observer, using (28).

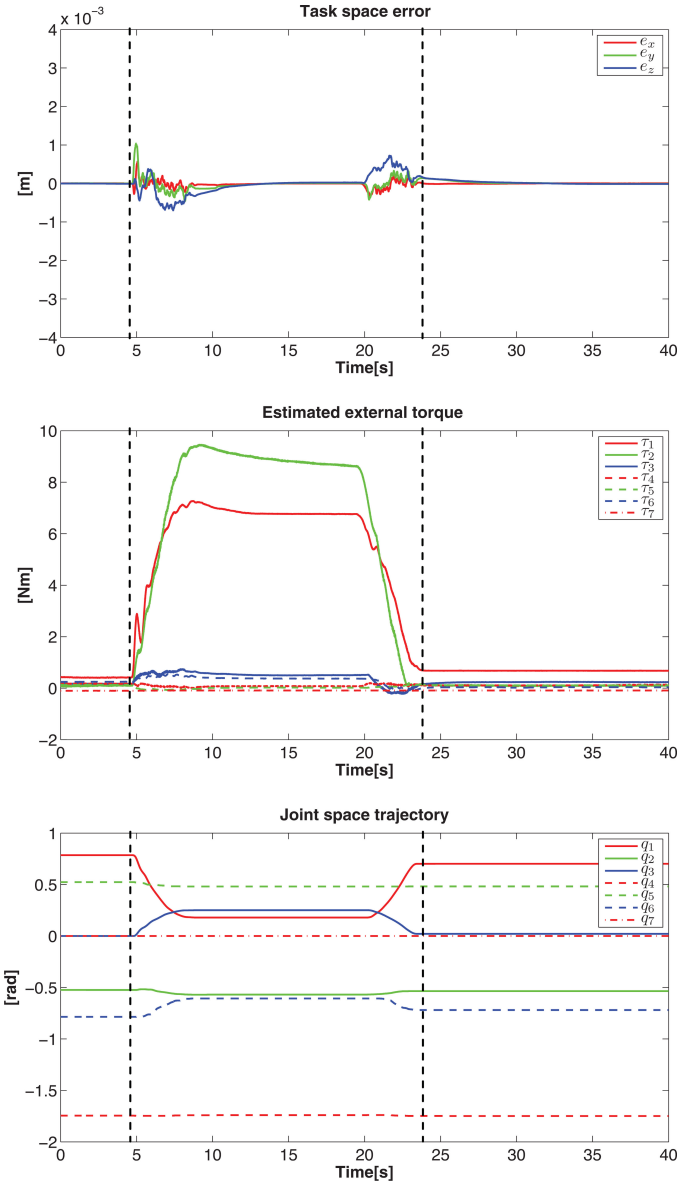

Fig. 5. Experiment 1: Task errors, external torques estimation evaluated from torque sensors and joint space trajectory, using task error-based observer.

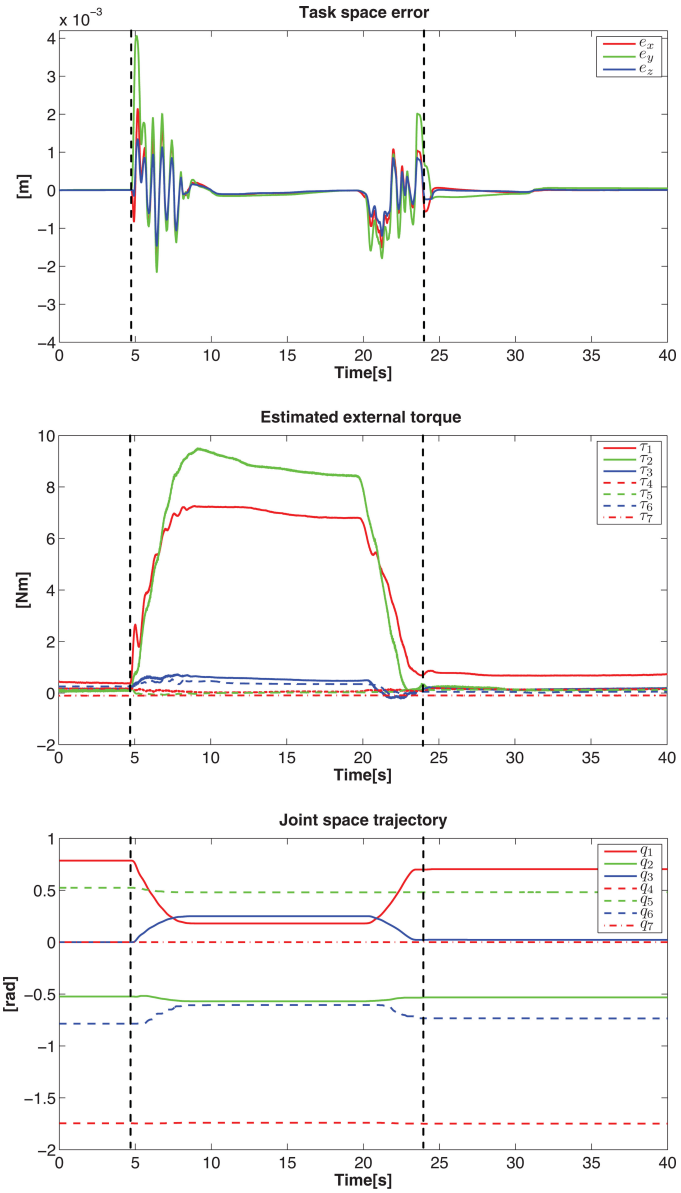

Fig. 6. Experiment 1: Task errors, external torques estimation evaluated from torque sensors and joint space trajectory, using momentum-based observer.

and the third phase of the interaction, namely, when the sphere is approached and retreated, the controller performs very well and the task errors is more than three times lower than the previous case, and the resulting interaction torques remain bounded. In the second phase of the interaction, when the sphere is at rest and a constant torque is applied, the task error converges to zero.

The experiment also has been performed using command acceleration (48) with the disturbance observer (49). The results are similar to Fig. 5 and, thus, have not been reported here.

Comparing the plots of the time histories of the external torques and of the joint positions in Figs. 3 and 5, it can be inferred that the behavior of the robot in the null space does not change appreciably. Moreover, comparing the task-space errors of Fig. 5 with those reported in Figs. 3 and 4, it can be observed that the control scheme with task error-based observer not only reduces the error during the interaction but reduces the effects of friction as well so that the task-space error goes to zero when the contact is lost.

Case III—Interaction Control With the Momentum-Based Observer: The experiment is repeated using the momentum-based observer (55) and the command acceleration (58). The gains have been set as $\boldsymbol{K}_p = 2000\boldsymbol{I}$, $\boldsymbol{K}_v = 90\boldsymbol{I}$, and $\boldsymbol{K}_I = 8\boldsymbol{I}$.

The results are depicted in Fig. 6. For completeness, in Fig. 7, the time history of the residual vector $\boldsymbol{r}$ is reported as well. It can be seen that the controller works very well during the constant phase of the interaction. However, when the external torque is not constant, during the first and the third phase of the interaction, the task-space error shows high-frequency oscillations.

This behavior can be mitigated using the PD+ command acceleration (71) as suggested in Remark 3. The task-space error for this case is reported in Fig. 8. It can be seen that the performance of the system, during the first and third phase of

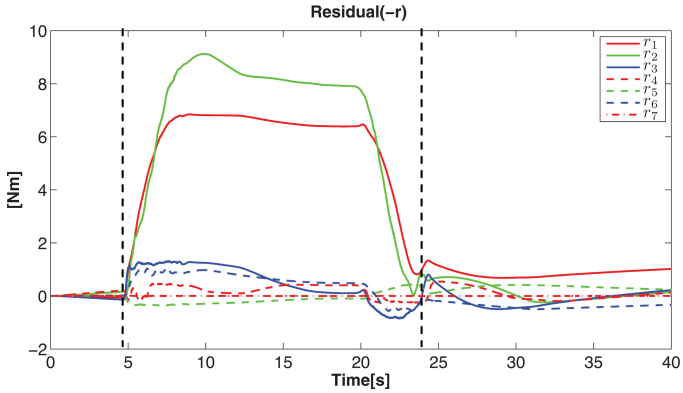

Fig. 7. Experiment 1: Residual vector using momentum-based observer with command acceleration (71).

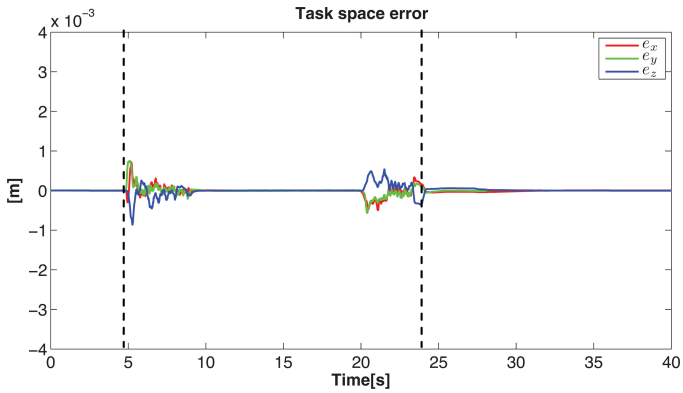

Fig. 8. Experiment 1: Task errors using momentum-based observer with command acceleration (71).

the interaction, is improved. The estimated external torque and the joint space trajectory do not change significantly and are not reported here for brevity.

B. Experiment 2

In the second set of experiments, the performance of the schemes considered previously are tested in a scenario in which the end effector of the robot follows a trajectory in the task space, and the body of the robot experiences a contact with a vertical wall in a point close to the fourth joint, as depicted in Fig. 9. Clearly, in this case, both task-space control and safety during contact are required. To increase safety and protect the body of the robot from any damage during the experiment, the wall is covered with a soft pad.

The experiment has been performed using the control laws (20) and (21) with the command accelerations considered in the previous section, namely, the scheme with no observer (Case I), the scheme with task error-based observer (Case II), and the scheme with momentum-based observer (Case III). The specific control laws and the corresponding gains are collected in Table I. Notice that, to improve the tracking capability in the task space, the command accelerations (29) and (58) have been suitably modified by adding feedforward of the desired task-space velocity and acceleration. The modified control laws can be easily derived and are not reported for brevity.

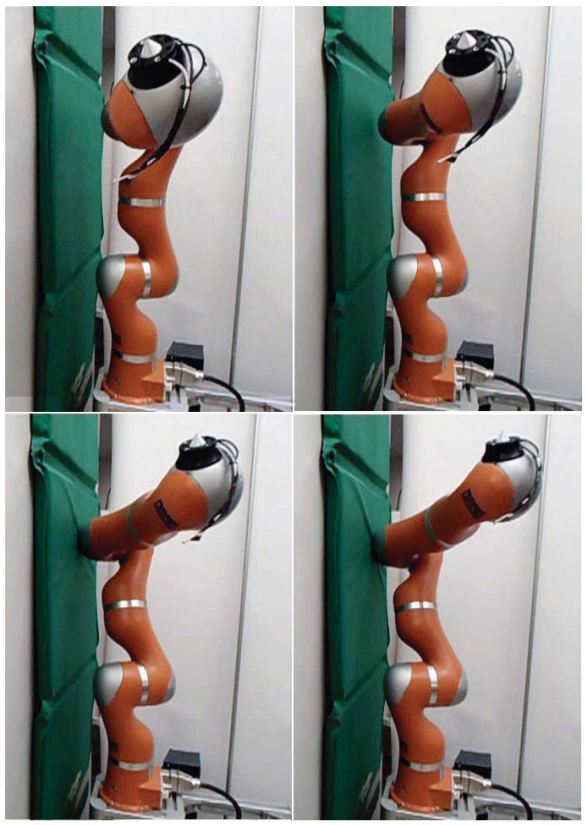

Fig. 9. Experiment 2: Snapshot of the KUKA LWR4 robot in contact with a wall.

TABLE I
EXPERIMENT 2

Case	Command Acc.	Controller Parameters
I	(26), (31)	$\boldsymbol{K}_p = 3000, \boldsymbol{K}_v = 110$ $\boldsymbol{B}_\nu = 0.4\boldsymbol{I}, \boldsymbol{K}_d = 5.6\boldsymbol{I}$
II	(29), (30), (31)	$\boldsymbol{P} = 25\boldsymbol{I}, \boldsymbol{K} = 80\boldsymbol{I}, \boldsymbol{\Gamma}_f = 0.063\boldsymbol{I}$ $\boldsymbol{B}_\nu = 0.4\boldsymbol{I}, \boldsymbol{K}_d = 5.6\boldsymbol{I}$
III	(58), (55), (31)	$\boldsymbol{K}_p = 3000\boldsymbol{I}, \boldsymbol{K}_v = 110\boldsymbol{I}, \boldsymbol{K}_I = 5\boldsymbol{I}$ $\boldsymbol{B}_\nu = 0.4\boldsymbol{I}, \boldsymbol{K}_d = 5.6\boldsymbol{I}$

The trajectory is a straight line motion from $\boldsymbol{x}_i = [0.01, -0.44, 0.76]^T$ to $\boldsymbol{x}_f = [0.12, -0.16, 0.85]^T$ and is planned according to a fifth-order polynomial of time, with duration 10 s. Then, the robot is kept in the final position for other 10 s. A constant configuration $\boldsymbol{q}_d = [3\pi/4, -\pi/6, 0, -\pi/1.8, \pi/6, -\pi/4, 0]^T$, which is consistent with the initial position $\boldsymbol{x}_i$, is considered as the desired goal in the null space. The vertical wall is located such that the contact with the wall starts at about $t = 4.5$ s.

It is worth remarking that the stability in this paper has been demonstrated only for the regulation case, due to the complexity of the analysis for the tracking case. Moreover, the desired joint configuration is consistent only with the initial position of the robot. This way, the robot executes the assigned task while keeping a joint configuration as close as possible to the initial configuration. Indeed, the purpose of this experiment is that of

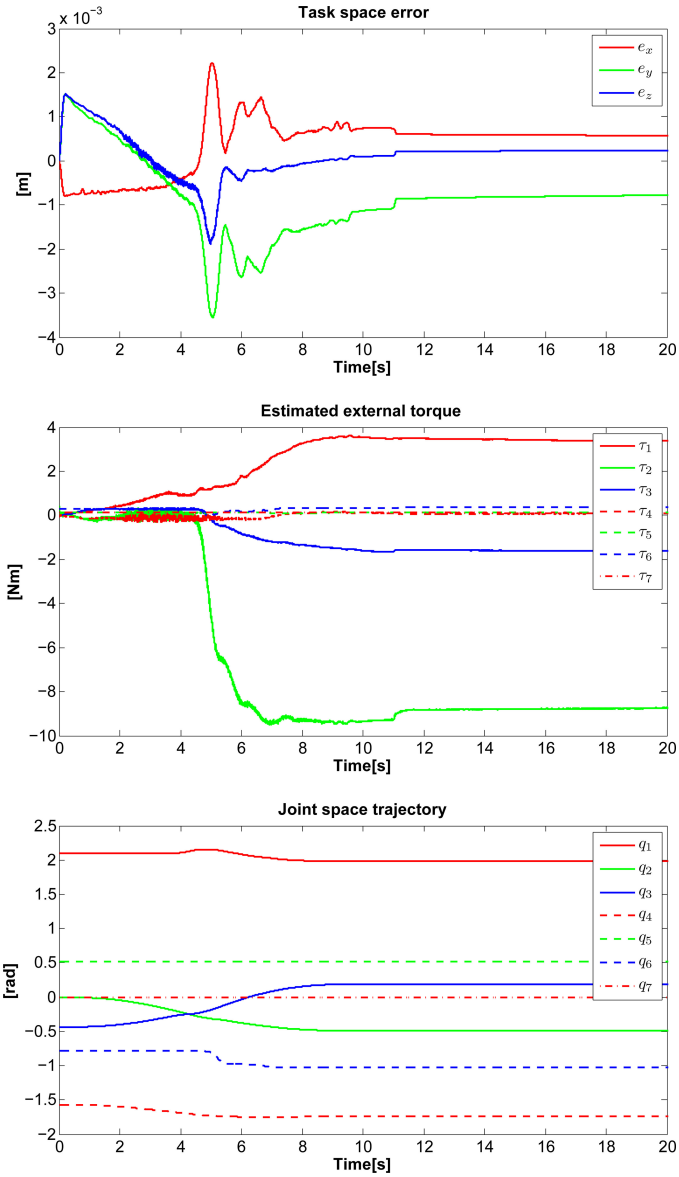

Fig. 10. Experiment 2: Task errors, external torques estimation evaluated from torque sensors and joint space trajectory, with no observer.

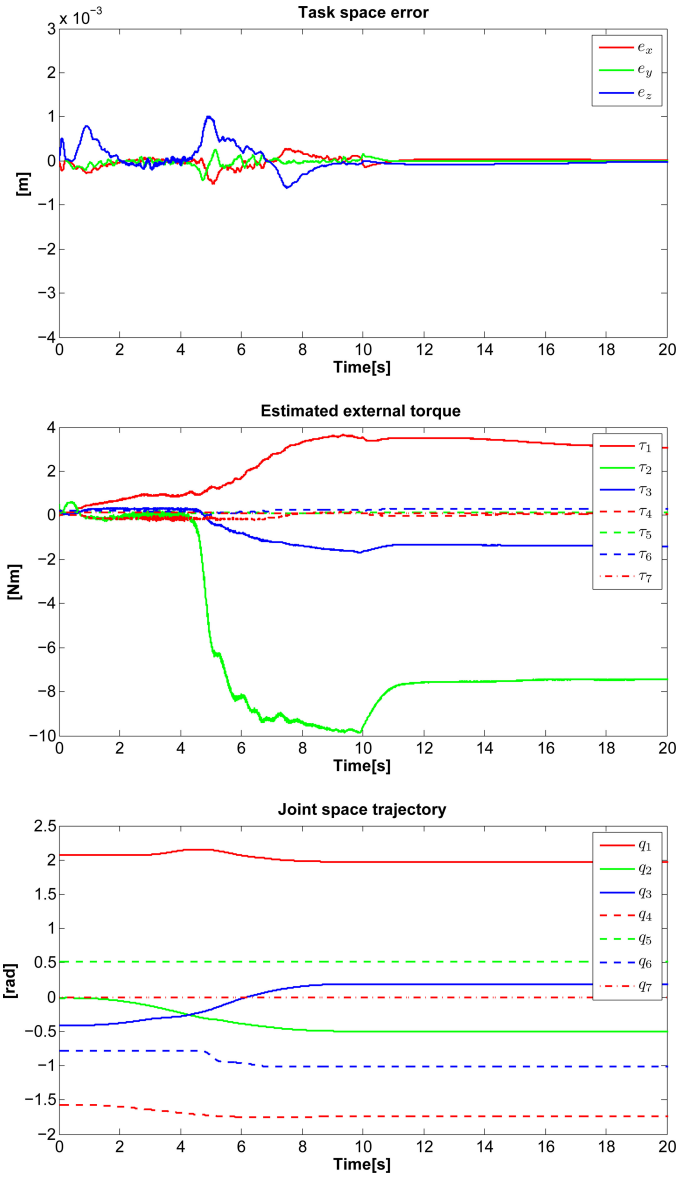

Fig. 11. Experiment 2: Task errors, external torques estimation evaluated from torque sensors, and joint space trajectory, using task error-based observer.

testing the performance of the proposed algorithms, also in a more complex and realistic scenario.

The performance of the controllers are shown in Figs. 10–12. It can be seen that, using the schemes with the observers (see Figs. 11 and 12), the task-space error can be considerably reduced with respect to the control schemes with no observer (see Fig. 10). Moreover, the robot body complies after contact with the wall so that the external toques remain limited. As in the previous experiment, the time histories of joint external torques, as well as those of the joint variables, are very similar for the different controllers, due to the fact that the null-space impedance dynamics is the same for all the controllers.

C. Discussion

Differently from the task error-based observer, the residual observer allows the estimation of the full external torque applied to the robot. Moreover, the computation of the residual (55) does not depend on the particular control law and can be useful also for other applications, e.g., collision detection. The price to pay is the dependence of (55) on the complete dynamic model of the robot.

On the other hand, experiments carried out neglecting the effect of Coriolis/centrifugal forces and assuming uncertainty in the inertial parameters of the system up to 50% show acceptable performance for both the approaches. Moreover, in the case of the observer based on the task error, and for slowly time-varying desired trajectory, the control law can be simplified as

$$\boldsymbol{\tau} = \boldsymbol{J}^T(\boldsymbol{D}\dot{\boldsymbol{x}} + \boldsymbol{K}\tilde{\boldsymbol{x}} + \boldsymbol{J}^{\#T}\,\widehat{\boldsymbol{\tau}}) + \boldsymbol{\tau}_{\text{null}} + \boldsymbol{g}(\boldsymbol{q}) \qquad (73)$$

where $\widehat{\boldsymbol{\tau}}$ is given by (49), and $\boldsymbol{\tau}_{\text{null}}$ is the torque related to null space computed as in (34). Our experiments, which are

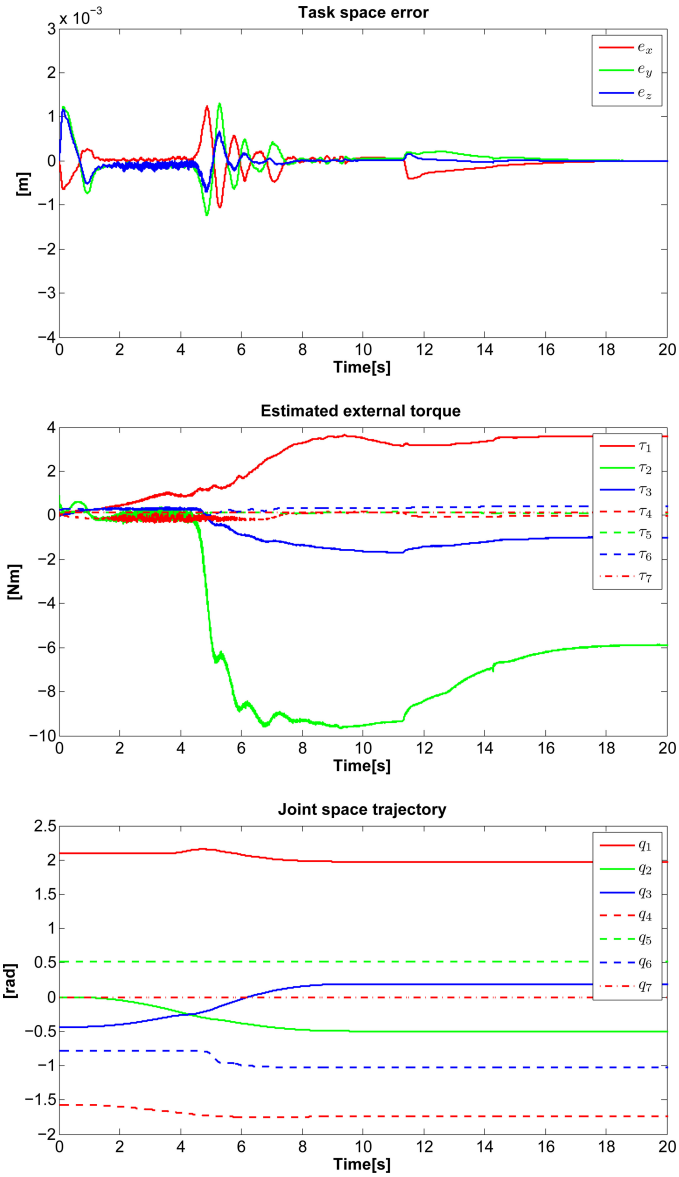

Fig. 12. Experiment 2: Task errors, external torques estimation evaluated from torque sensors and joint space trajectory, using momentum-based observer.

not presented here, show that the performance of the controller remains still acceptable.

Another issue confirmed by experiments that are not shown here for brevity, is that, as it was discussed in Remark 1, the non-minimal representation for the null-space control $\boldsymbol{\tau}_{\text{null}}$ can also be used with a little degradation of the performance with respect to the minimal case. The only significant difference that was noticed experimentally is that, by adopting a minimal representation for the null-space control, higher gains in the task-space control can be used. Notice that it is well established that the non-minimal representation of null-space control is stable in the presence of null-space velocity feedback (see, e.g., [36] and [44]), but no theoretical results are available for the case of more complex control algorithms as impedance control. On the other hand, as proven in [45], minimal null-space-based control algorithms ensure stable operation for general torque-based null-space control.

It is worth observing that, to avoid dangerous situations, the assigned task should be relaxed based on the amount of exchanged forces. In other words, the main task should be preserved only when the estimated forces are below a suitable safety threshold.

Finally, it is clear that the effectiveness of the algorithm relies on the number of available degrees of redundancy. If required, depending on the task, the number of constrained task variables can be decreased in order to increase the dimension of the null space where compliance is ensured.

VI. Conclusion

Two nonlinear controller–observer approaches that ensure task-space error convergence, besides proper compliant behavior in the null space, have been presented. The controllers do not need torque sensors and can be used for the case where the robot works, for instance, in human environments, and the interaction with the robot body can occur intentionally or accidentally. Under these conditions, the redundancy of the system is utilized to ensure safe and dependable physical interaction, while the main task is preserved. The first approach is based on task-space information, and the second one acts based on the generalized momentum of the system. The stability of the whole system was shown by using the concept of conditional stability. The experimental results obtained from a torque-controlled KUKA LWR4 robot confirm the theoretical findings.

Appendix A
Dynamics Model in the Task Space and the Null Space

Task-space dynamics and null-space dynamics can be obtained multiplying both sides of (1) by $\boldsymbol{J}_E^{-T}$. This gives

$$\boldsymbol{\Lambda}_E(\boldsymbol{q})\begin{pmatrix}\ddot{\boldsymbol{x}}\\ \dot{\boldsymbol{\nu}}\end{pmatrix}+\boldsymbol{\mu}_E(\boldsymbol{q},\dot{\boldsymbol{q}})\begin{pmatrix}\dot{\boldsymbol{x}}\\ \boldsymbol{\nu}\end{pmatrix}+\boldsymbol{J}_E^{-T}\boldsymbol{g}(\boldsymbol{q})+\begin{pmatrix}\boldsymbol{F}_{x,\text{ext}}\\ \boldsymbol{F}_{v,\text{ext}}\end{pmatrix}=\begin{pmatrix}\boldsymbol{F}_x\\ \boldsymbol{F}_\nu\end{pmatrix} \quad (74)$$

where

$$\boldsymbol{\Lambda}_E(\boldsymbol{q})=\boldsymbol{J}_E^{-T}\boldsymbol{M}\boldsymbol{J}_E^{-1}=\begin{pmatrix}\boldsymbol{\Lambda}_x & \boldsymbol{0}\\ \boldsymbol{0} & \boldsymbol{\Lambda}_\nu\end{pmatrix}$$
$$\boldsymbol{\Lambda}_x(\boldsymbol{q})=(\boldsymbol{J}\boldsymbol{M}^{-1}\boldsymbol{J}^T)^{-1}$$
$$\boldsymbol{\Lambda}_\nu(\boldsymbol{q})=\boldsymbol{Z}^T\boldsymbol{M}\boldsymbol{Z} \quad (75)$$

and

$$\boldsymbol{\mu}_E(\boldsymbol{q},\dot{\boldsymbol{q}})=\begin{pmatrix}\boldsymbol{\mu}_x & \boldsymbol{\mu}_{xv}\\ \boldsymbol{\mu}_{vx} & \boldsymbol{\mu}_\nu\end{pmatrix}$$
$$\boldsymbol{\mu}_x(\boldsymbol{q},\dot{\boldsymbol{q}})=(\boldsymbol{J}^{\#T}\boldsymbol{C}(\boldsymbol{q},\dot{\boldsymbol{q}})-\boldsymbol{\Lambda}_x\dot{\boldsymbol{J}})\boldsymbol{J}^{\#}$$
$$\boldsymbol{\mu}_{xv}(\boldsymbol{q},\dot{\boldsymbol{q}})=(\boldsymbol{J}^{\#T}\boldsymbol{C}(\boldsymbol{q},\dot{\boldsymbol{q}})-\boldsymbol{\Lambda}_x\dot{\boldsymbol{J}})\boldsymbol{Z}$$
$$\boldsymbol{\mu}_\nu(\boldsymbol{q},\dot{\boldsymbol{q}})=(\boldsymbol{Z}^T\boldsymbol{C}(\boldsymbol{q},\dot{\boldsymbol{q}})-\boldsymbol{\Lambda}_\nu\dot{\boldsymbol{Z}}^{\#})\boldsymbol{Z}$$
$$\boldsymbol{\mu}_{vx}(\boldsymbol{q},\dot{\boldsymbol{q}})=(\boldsymbol{Z}^T\boldsymbol{C}(\boldsymbol{q},\dot{\boldsymbol{q}})-\boldsymbol{\Lambda}_\nu\dot{\boldsymbol{Z}}^{\#})\boldsymbol{J}^{\#}. \quad (76)$$

The projected forces acting on the task space and the null space are related to the joint space torques through the following equalities:

$$\begin{pmatrix} \boldsymbol{F}_{x,\mathrm{ext}} \\ \boldsymbol{F}_{v,\mathrm{ext}} \end{pmatrix} = \boldsymbol{J}_E^{-T}\boldsymbol{\tau}_{\mathrm{ext}} = \begin{pmatrix} \boldsymbol{J}^{\#T}\boldsymbol{\tau}_{\mathrm{ext}} \\ \boldsymbol{Z}^T\boldsymbol{\tau}_{\mathrm{ext}} \end{pmatrix} \tag{77}$$

$$\begin{pmatrix} \boldsymbol{F}_x \\ \boldsymbol{F}_\nu \end{pmatrix} = \boldsymbol{J}_E^{-T}\boldsymbol{\tau} = \begin{pmatrix} \boldsymbol{J}^{\#T}\boldsymbol{\tau} \\ \boldsymbol{Z}^T\boldsymbol{\tau} \end{pmatrix}. \tag{78}$$

Note that because of the particular choice of $\boldsymbol{Z}^{\#}$, $\boldsymbol{\Lambda}_E(\boldsymbol{q})$ is block diagonal, and thus, the task-space dynamic and the null-space dynamic are inertially decoupled [30]. It can be shown that matrix $\boldsymbol{\Lambda}_E$ is symmetric and positive definite, and so are $\boldsymbol{\Lambda}_x$ and $\boldsymbol{\Lambda}_\nu$. Moreover, $\dot{\boldsymbol{\Lambda}}_E - 2\boldsymbol{\mu}_E$ is skew-symmetric, if $\dot{\boldsymbol{M}} - 2\boldsymbol{C}$ is skew-symmetric. This, in turn, implies that, $\boldsymbol{\mu}_{vx} = -\boldsymbol{\mu}_{xv}^T$ and both the matrices $\dot{\boldsymbol{\Lambda}}_x - 2\boldsymbol{\mu}_x$ and $\dot{\boldsymbol{\Lambda}}_\nu - 2\boldsymbol{\mu}_\nu$ are skew-symmetric.

APPENDIX B
SOLUTION OF (47)

It is not difficult to show (see, e.g., [43]) that the equations

$$\boldsymbol{Z}(\boldsymbol{q})^T(\boldsymbol{K}_d\tilde{\boldsymbol{q}} - \boldsymbol{\tau}_{\mathrm{ext}}) = \boldsymbol{0} \tag{79}$$

$$\boldsymbol{x}(\boldsymbol{q}) = \boldsymbol{x}_d \tag{80}$$

where $\boldsymbol{q}_d$ is an assigned nonsingular joint configuration, $\tilde{\boldsymbol{q}} = \boldsymbol{q}_d - \boldsymbol{q}$, and the $\boldsymbol{K}_d$ diagonal and positive-definite matrix are the necessary conditions for the solutions of the constrained minimization problem

$$\min_{\boldsymbol{q}} \|\boldsymbol{K}_d\tilde{\boldsymbol{q}} - \boldsymbol{\tau}_{\mathrm{ext}}\|^2 \tag{81}$$

subject to (80). This physically means that the manipulator, when a constant external torque $\boldsymbol{\tau}_{\mathrm{ext}}$ is applied, reaches a joint configuration $\boldsymbol{q}^*$ compatible with the main task $\boldsymbol{x}_d = \boldsymbol{x}(\boldsymbol{q})$, which minimize the elastic potential energy in (81).

In the case $\boldsymbol{\tau}_{\mathrm{ext}} = \boldsymbol{0}$, if $\boldsymbol{q}_d$ is compatible to $\boldsymbol{x}_d$, i.e., $\boldsymbol{x}(\boldsymbol{q}_d) = \boldsymbol{x}_d$, then a solution to (79) and (80) is $\tilde{\boldsymbol{q}} = \boldsymbol{0}$. This solution is an isolated point. This can be easily proven by contradiction. In fact, if $\tilde{\boldsymbol{q}} = \boldsymbol{0}$ is not an isolated point, then there exists an infinitesimal displacement $d\boldsymbol{q} \neq \boldsymbol{0}$ such that $\bar{\boldsymbol{q}} = \boldsymbol{q}_d + d\boldsymbol{q}$ satisfies (79) and (80) with $\tilde{\boldsymbol{q}} = -d\boldsymbol{q}$. In a first-order approximation, it is $\boldsymbol{Z}^T(\boldsymbol{q}_d + d\boldsymbol{q})\boldsymbol{K}_d d\boldsymbol{q} \approx \boldsymbol{Z}^T(\boldsymbol{q}_d)\boldsymbol{K}_d d\boldsymbol{q}$ and $\boldsymbol{x}(\bar{\boldsymbol{q}}) \approx \boldsymbol{x}(\boldsymbol{q}_d) + \boldsymbol{J}(\boldsymbol{q}_d)d\boldsymbol{q}$. Hence, in view of (79) and (80), $d\boldsymbol{q}$ must satisfy both the equations $\boldsymbol{Z}^T(\boldsymbol{q}_d)\boldsymbol{K}_d d\boldsymbol{q} = \boldsymbol{0}$ and $\boldsymbol{J}(\boldsymbol{q}_d)d\boldsymbol{q} = \boldsymbol{0}$. Since $\boldsymbol{q}_d$ is a nonsingular configuration, considering that the columns of $\boldsymbol{K}_d\boldsymbol{Z}$ span the null space of matrix $\boldsymbol{J}$ (being $\boldsymbol{K}_d$ a diagonal matrix), the only solution to both these equations is $d\boldsymbol{q} = \boldsymbol{0}$.

REFERENCES

[1] H. Sadeghian, M. Keshmiri, L. Villani, and B. Siciliano, "Null-space impedance control with disturbance observer," in *Proc. IEEE/RSJ Int. Conf. Intell. Robots Syst.*, 2012, pp. 2795–2800.

[2] A. De Santis, B. Siciliano, A. D. Luca, and A. Bicchi, "An atlas of physical human-robot interaction," *Mech. Mach. Theory*, vol. 43, pp. 253–270, 2008.

[3] A. De Luca, A. Albu-Schaffer, S. Haddadin, and G. Hirzinger, "Collision detection and safe reaction with the DLR-III lightweight robot arm," in *Proc. IEEE/RSJ Int. Conf. Intell. Robots Syst.*, 2006, pp. 1623–1630.

[4] S. Haddadin, A. Albu-Schaffer, A. De Luca, and G. Hirzinger, "Collision detection and reaction: A contribution to safe physical human-robot interaction," in *Proc. IEEE/RSJ Int. Conf. Intell. Robots Syst.*, 2008, pp. 3356–3363.

[5] A. C. Smith, F. Mobasser, and K. Hashtrudi-Zaad, "Neural-network-based contact force observers for haptic applications," *IEEE Trans. Robot.*, vol. 22, no. 6, pp. 1163–1175, Dec. 2006.

[6] A. D. Luca and R. Mattone, "Sensorless robot collision detection and hybrid force/motion control," in *Proc. IEEE Int. Conf. Robot. Autom.*, 2005, pp. 999–1004.

[7] A. D. Luca and L. Ferrajoli, "Exploiting robot redundancy in collision detection and reaction," in *Proc. IEEE/RSJ Int. Conf. Intell. Robots Syst.*, 2008, pp. 3299–3305.

[8] S. Haddadin, A. Albu-Schaffer, and G. Hirzinger, "Requirements for safe robots: Measurements, analysis and new insights," *Int. J. Robot. Res.*, vol. 28, pp. 1507–1527, 2009.

[9] A. Bicchi and G. Tonietti, "Fast and soft arm tactics: Dealing with the safety performance trade-off in robot arms design and control," *IEEE Robot. Autom. Mag.*, vol. 11, no. 2, pp. 22–33, Jun. 2004.

[10] D. Tsetserukou and N. Kawakami, "Design, control and evaluation of a whole-sensitive robot arm for physical human-robot interaction," *Int. J. Human. Robot.*, vol. 6, no. 4, pp. 699–725, 2009.

[11] A. Albu-Schaffer and G. Hirzinger, "Cartesian impedance control techniques for torque controlled light-weight robots," in *Proc. IEEE Int. Conf. Robot. Autom.*, 2002, pp. 657–663.

[12] B. Siciliano and L. Villani, "An inverse kinematics algorithm for interaction control of a flexible arm with a compliant surface," *Control Eng. Practice*, vol. 9, no. 2, pp. 191–198, 2001.

[13] F. Caccavale, P. Chiacchio, A. Marino, and L. Villani, "Six-DOF impedance control of dual-arm cooperative manipulators," *IEEE/ASME Trans. Mechatronics*, vol. 13, no. 5, pp. 576–586, Oct. 2008.

[14] V. Lippiello, B. Siciliano, and L. Villani, "A position-based visual impedance control for robot manipulators," in *Proc. IEEE Int. Conf. Robot. Autom.*, 2007, pp. 2068–2073.

[15] D. Tsetserukou, N. Kawakami, and S. Tachi, "iSoRA: Humanoid robot arm for intelligent haptic interaction with the environment," *Adv. Robot.*, vol. 23, pp. 1327–1358, 2009.

[16] Y. Li, S. S. Ge, and C. Yang, "Impedance control for multi-point human robot interaction," in *Proc. 8th Asian Control Conf.*, 2011, pp. 1187–1192.

[17] Y. Li, S. S. Ge, C. Yang, X. Li, and K. P. Tee, "Model-free impedance control for safe human robot interaction," in *Proc. IEEE Int. Conf. Robot. Autom.*, 2011, pp. 6021–6026.

[18] Y. Li, S. S. Ge, and C. Yang, "Learning impedance control for physical robot-environment interaction," *Int. J. Control*, vol. 85, no. 2, pp. 182–193, 2012.

[19] C. Ott, "Cartesian impedance control of redundant and flexible joint robots," in *Springer Tracts in Advanced Robotics*, vol. 49. New York, NY, USA: Springer, 2008.

[20] A. Albu-Schaffer, C. Ott, U. Frese, and G. Hirzinger, "Cartesian impedance control of redundant robots; recent results with the DLR-Light-Weight arms," in *Proc. IEEE Int. Conf. Robot. Autom.*, 2003, pp. 3704–3709.

[21] A. Albu-Schaffer, C. Ott, and G. Hirzinger, "A unified passivity based control framework for position, torque and impedance control of flexible joint robots," *Int. J. Robot. Res.*, vol. 26, pp. 23–39, 2007.

[22] J. Nakanishi, R. Cory, M. J. Peters, and S. Schaal, "Operational space control: A theoretical and empirical comparison," *Int. J. Robot. Res.*, vol. 27, pp. 737–757, 2008.

[23] Y. Nakamura, *Advanced Robotics: Redundancy and Optimization*. New York, NY, USA: Addison-Wesley, 1991.

[24] B. Siciliano and J. J. Slotine, "A general framework for managing multiple tasks in highly redundant robotic systems," in *Proc. 5th Int. Conf. Adv. Robot.*, 1991, vol. 2, pp. 1211–1216.

[25] O. Khatib, L. Sentis, J. H. Park, and J. Warren, "Whole-body dynamic behavior and control of human-like robots," *Int. J. Human. Robot.*, vol. 1, pp. 29–43, 2004.

[26] H. Sadeghian, L. Villani, M. Keshmiri, and B. Siciliano, "Multi-priority control in redundant robotic systems," in *Proc. IEEE/RSJ Int. Conf. Intell. Robots Syst.*, 2011, pp. 3752–3757.

[27] R. Platt, Jr., M. Abdallah, and C. Wampler, "Multiple priority Cartesian impedance control," presented at the Robot.: Sci. Syst. Conf., Zaragoza, Spain, 2010.

[28] R. Platt, Jr., M. Abdallah, and C. Wampler, "Multiple priority impedance control," in *Proc. IEEE Int. Conf. Robot. Autom.*, 2011, pp. 6033–6038.
[29] M. Diftler, J. Mehling, M. Abdallah, N. Radford, L. Bridgwater, A. Sanders, S. Askew, M. Linn, J. Yamokoski, F. Permenter, B. Hargrave, R. Platt, R. Savely, and R. Ambrose, "Robonaut 2—The first humanoid robot in space," in *Proc. IEEE Int. Conf. Robot. Autom.*, 2011, pp. 2178–2183.
[30] Y. Oh, W. Chung, and Y. Youm, "Extended impedance control of redundant manipulators based on weighted decomposition of joint space," *J. Robot. Syst.*, vol. 15, no. 5, pp. 231–258, 1998.
[31] A. De Luca and G. Oriolo, "Nonholonomic behavior in redundant robots under kinematic control," *IEEE Trans. Robot. Autom.*, vol. 13, no. 5, pp. 776–782, Oct. 1997.
[32] C. Ott, A. Kugi, and Y. Nakamura, "Resolving the problem of non-integrability of null-space velocities for compliance control of redundant manipulators by using semi-definite Lyapunov functions," in *Proc. IEEE Int. Conf. Robot. Autom.*, 2008, pp. 1999–2004.
[33] A. Parmiggiani, M. Randazzo, L. Natale, G. Metta, and G. Sandini, "Joint torque sensing for the upper-body of the iCub humanoid robot," in *Proc. 9th IEEE-RAS Int. Conf. Human. Robots*, 2009, pp. 15–20.
[34] B. Siciliano, L. Sciavicco, L. Villani, and G. Oriolo, *Robotics: Modelling, Planning and Control*. New York, NY, USA: Springer-Verlag, 2009.
[35] O. Khatib, "Inertial properties in robotic manipulation: An object-level framework," *Int. J. Robot. Res.*, vol. 14, no. 1, pp. 19–36, 1995.
[36] B. Nemec, L. Zlajpah, and D. Omrcen, "Comparison of null-space and minimal null-space control algorithms," *Robotica*, vol. 25, pp. 511–520, 2007.
[37] F. Caccavale, C. Natale, B. Siciliano, and L. Villani, "Resolved acceleration control of robot manipulators: A critical review with experiments," *Robotica*, vol. 16, pp. 565–573, 1998.
[38] A. Iggidr and G. Sallet, "On the stability of nonautonomous systems," *Automatica*, vol. 39, pp. 167–171, 2003.
[39] B. Paden and R. Panja, "Globally asymptotically stable PD+ controller for robot manipulators," *Int. J. Control*, vol. 47, no. 6, pp. 1697–1712, 1988.
[40] V. Santibanez and R. Kelly, "Strict Lyapunov functions for control of robot manipulators," *Automatica*, vol. 33, no. 4, pp. 675–682, 1997.
[41] H. K. Khalil, *Nonlinear Systems*, 3rd ed. Englewood Cliffs, NJ, USA: Prentice-Hall, 2002.
[42] G. Schreiber, A. Stemmer, and R. Bischoff, "The fast research interface for the KUKA lightweight robot," in *Proc. IEEE Int. Conf. Robot. Autom., Workshop Innovat. Robot Contr. Architect. Demand. (Res.) Appl.*, 2010, pp. 15–21.
[43] P. Chang, "A closed-form solution for inverse kinematics of robot manipulators with redundancy," *IEEE J. Robot. Autom.*, vol. RA-3, no. 5, pp. 393–403, Oct. 1987.
[44] C. Natale, B. Siciliano, and L. Villani, "Spatial impedance control of redundant manipulators," in *Proc. IEEE Int. Conf. Robot. Autom.*, 1999, pp. 1788–1793.
[45] J. Park, W. Chung, and Y. Youm, "Characterization of instability of dynamic control for kinematically redundant manipulators," in *Proc. IEEE Conf. Robot. Autom.*, 2002, pp. 2400–2405.

Hamid Sadeghian was born in Isfahan, Iran, in 1982. He received the B.Sc. and M.Sc. degrees in mechanical engineering from the Isfahan University of Technology and the Sharif University of Technology, Tehran, Iran, in 2005 and 2008, respectively. He received the Ph.D. degree in mechanical engineering (robotics and control) from the Isfahan University of Technology in 2013.

From November 2010 to January 2013, he was a Visiting Scholar with the PRISMA Laboratory, Department of Electrical Engineering and Information Technology, University of Naples, Naples, Italy. He is currently an Assistant Professor with the Department of Biomedical Engineering, Faculty of Engineering, University of Isfahan. His research interests include physical human–robot interaction, impedance control, redundant manipulation, and nonlinear control of mechanical systems.

Luigi Villani (S'94–M'97–SM'03) was born in Avellino, Italy, in 1966. He received the *Laurea* degree in electronic engineering and the Research Doctorate degree in electronic engineering and computer science from the University of Naples, Naples, Italy, in 1992 and 1996, respectively.

He is currently an Associate Professor of automatic control with the Department of Electrical Engineering and Information Technology, University of Naples. His research interests include force/motion control of manipulators, safe physical human–robot interaction, cooperative robot manipulation, lightweight flexible arms, adaptive and nonlinear control of mechanical systems, visual servoing, fault diagnosis, and fault tolerance for dynamical systems. He has coauthored six books, 50 journal papers, and more than 100 conference papers and book chapters.

Dr. Villani was an Associate Editor of IEEE TRANSACTIONS ON ROBOTICS from 2007 to 2011 and IEEE TRANSACTIONS ON CONTROL SYSTEMS TECHNOLOGY from 2005 to 2012.

Mehdi Keshmiri was born in Natanz, Iran, in 1961. He received the B.Sc. and M.Sc. degree in mechanical engineering from the Sharif University of Technology, Tehran, Iran, in 1986 and 1989, respectively. He received the Ph.D. degree in mechanical engineering (space dynamics) from McGill University, Montreal, QC, Canada, in 1995.

He then joined the Isfahan University of Technology, Isfahan, Iran, where he is currently an Associate Professor with the Department of Mechanical Engineering. His research interests include system dynamics, control systems and dynamics, and control of robotic systems. He has presented and published more than 100 papers in international conferences and journals and supervised more than 60 Ph.D. and Master's students.

Bruno Siciliano (M'91–SM'94–F'00) was born in Napoli, Italy, in 1959. He received the Laurea degree and the Research Doctorate degree in electronic engineering from the University of Naples, Naples, Italy, in 1982 and 1987, respectively.

He is currently a Professor of control and robotics and the Director of the PRISMA Laboratory with the Department of Electrical Engineering and Information Technology, University of Naples Federico II, Naples, Italy. His research interests include force and visual control, human–robot interaction, and service robotics. He has coauthored seven books, 70 journal papers, 170 conference papers, and several book chapters. He has delivered 100 invited lectures and seminars at institutions worldwide, and he has been the recipient of several awards.

Dr. Siciliano is a Fellow of the American Society of Mechanical Engineers and the International Federation of Automatic Control. He has served on the editorial boards of several peer-reviewed journals and has been Chair of program and organizing committees of several international conferences. He is the coeditor of the *Springer Tracts in Advanced Robotics* and of the *Springer Handbook of Robotics*, which received the PROSE Award for Excellence in Physical Sciences and Mathematics and was also the winner in the category Engineering and Technology. His group has been granted 13 European projects, including an ERC Advanced Grant. He is the Past President of the IEEE Robotics and Automation Society.